

New results on vacuum fluctuations: Accelerated detector versus inertial detector in a quantum field

I-Chin Wang

Institute of Physics, Academia Sinica, Taipei 11529, Taiwan

We investigate the interaction between a moving detector and a quantum field, especially about how the trajectory of the detector would affect the vacuum fluctuations when the detector is moves in a quantum field (the Unruh effect). We focus on two moving detectors system for future application in quantum teleportation. We find that the trajectory of a uniformly accelerated detector in Rindler space cannot be extended to a trajectory in which a detector moves at constant velocity. Based on our previous work, we redo the calculations and find that a term is missing from the past calculations, and we also find that there are some restrictions on the values for the parameters in the solutions. In addition, without inclusion of the missing term, the variance from the quantum field for the inertial detector will be zero and is unlikely in such a system. When all these points are combined, there is a difference in the two-point correlation function between the inertial detector and the accelerated detector in the early-time region. The influence of proper acceleration can be seen in the two-point correlation functions. This might play a role in the quantum teleportation process and be worth studying thoroughly.

PACS numbers: 04.62.+v, 04.70.Dy, 12.20.-m

I. INTRODUCTION

The Unruh effect was originally proposed for the study of Hawking radiation near a black hole [1], and it was found that an uniformly accelerated detector would experience a thermal bath at temperature $T_U = \frac{\hbar a}{2\pi c k_B}$, where a is the proper acceleration. It involves the interaction between the background quantum field and a moving detector which has constant acceleration. It is also known that the accelerating charges emit radiation. In the literature [2–9], many physicists were interested in learning whether there were any differences between the Unruh effect and the radiation from accelerated charges in the quantum field; for example, was the emitted radiation part of the energy flux in the Unruh effect? Later, this question was extended to the atom system and to whether an accelerated atom emits radiated energy? What was the connection to the Unruh effect? Hu and his collaborators worked on the minimal coupling model [10–13] and considered what roles the equilibrium condition and nonequilibrium condition play in the accelerated detector [10, 11, 13, 14]. In recent years, the kinds of influences between the moving detector and a background quantum field have been applied to certain quantum teleportation processes. However, the difference between an inertial trajectory and the uniformly accelerated trajectory for a moving detector is not obvious enough. If we could clearly see the effect about proper acceleration, it would be helpful to the understanding of some important systems, for example, the atomic optical and particle quantum field systems.

Based on the work in Refs. [10–15], we follow here the work of Lin and co-workers [16–18], and we recheck the computation of a uniformly accelerated detector (UAD) [16]. It was originally thought that the solution of a UAD [16] could be applied to the inertial detector case directly by taking the limit such that the proper acceleration $a \rightarrow 0$ (i.e. an inertial detector moves at a constant velocity and therefore has zero proper acceleration). However, when we check past results for two-point correlation functions for a UAD, we find that the previous solution cannot be applied to the inertial detector case by taking the limit $a \rightarrow 0$. As an inertial detector moves at constant velocity, we need to apply a real inertial trajectory. In fact, the original goal for our work was to apply the previous results [16, 17] in certain quantum teleportation processes, but some errors occurred when we did it, so we have to recheck our setup and calculations. Therefore, we start from the beginning, where we apply a real inertial trajectory and another uniformly accelerating trajectory for the moving detector, solving the solutions for these two trajectories and then comparing the difference on the two-point correlation functions between the inertial and uniformly accelerated detectors.

We find that a term is missing from previous two-point correlation functions and that it is about the vacuum fluctuations of the moving detector. Without this term, we would have a zero variance from the quantum field for the inertial detector. This was not noticed before. When we include this term, the strange zero variance issue disappears and the values of the two-point correlation functions also change. This change makes the difference between the inertial and accelerated detector more clear than in the previous results. Since we apply perturbations to solve the equations, assumptions about the perturbation method also set an allowed region for the values of the parameters

in the solutions. This restriction also affects the solutions for the two-point correlation functions. When these considerations are included, the difference between the inertial detector and accelerated detector is more obvious than ever.

To apply our present result to future work about Quantum teleportation, we consider two moving Unruh-DeWitt detectors in our present model [17]: Alice and Bob. We assume that Alice is static in space and Bob is moving in space. Bob's worldline has two different choices: one is the trajectory for a uniform acceleration, while the other is for a constant velocity motion. For simplicity, we focus here on the moving detector Bob and study the interaction between the quantum field and the internal degrees of freedom Q for detector Bob. We compute the two-point functions $\langle QQ \rangle_v$ and $\langle \dot{Q}\dot{Q} \rangle_v$ for the two different trajectories (i.e., $\langle QQ \rangle_v$ is the two-point function vacuum fluctuation of the internal degrees of freedom for Bob), and we then compare the plots of $\langle QQ \rangle_v$ and $\langle \dot{Q}\dot{Q} \rangle_v$ for the inertial and uniformly accelerating detectors. We find that these two different types of detectors have different effects on the curves for the two-point functions $\langle QQ \rangle_v$ and $\langle \dot{Q}\dot{Q} \rangle_v$ in the early-time region. Meanwhile, we also write detailed calculations and point out some key points in the calculations about obtaining $\langle QQ \rangle_v$ and $\langle \dot{Q}\dot{Q} \rangle_v$.

To demonstrate the importance of the allowed region on the values of the parameters in this model, we choose some improper values for the parameters in the model and calculate the two-point correlation functions. Improper values would lead to different trends for the two-point functions $\langle QQ \rangle_v$ and make the Unruh effect unclear.

This paper is organized as follows. In Sec. II we set up and introduce the model and the method, and some detailed derivations are placed in the appendixes. In Sec. III we focus on one detector and investigate the moving detector Bob in a quantum field and whether it moves at a constant acceleration or a constant velocity. We solve the solutions for two different trajectories for the detector Bob and compute the two-point correlation functions of internal degree of freedom Q of Bob. We then discuss the allowed values for the parameters in the solutions and do the numerical plots for the two-point functions of Q . Later, we compare the plots and determine the difference between the inertial detector and accelerated detector. Sec. IV is the summary.

II. MODEL

We consider two Unruh-DeWitt detectors Alice and Bob that are at different spatial points and in different states of motion. Each detector has an internal degree of freedom Q that interacts with a common scalar field Φ . Assuming that Alice is static and Bob is moving (Bob could be uniformly accelerated or could move at a constant velocity; we will calculate the solutions for these two cases later). The trajectories for Alice and Bob are $z_A^\mu(t)$ and $z_B^\mu(\tau)$, respectively. The action for this setup is as follows:

$$S = - \int d^4x \sqrt{-g} \frac{1}{2} \partial_\mu \Phi(x) \partial^\mu \Phi(x) + \int d\tau_A \frac{m_0}{2} \left[(\partial_A Q_A)^2 - \Omega_0^2 Q_A^2 \right] + \int d\tau_B \frac{m_0}{2} \left[(\partial_B Q_B)^2 - \Omega_0^2 Q_B^2 \right] + \lambda_0 \int d^4x \int dt Q_A(t) \Phi(x) \delta^4(x^\mu - z_A^\mu(t)) + \lambda_0 \int d^4x \int d\tau Q_B(\tau) \Phi(x) \delta^4(x^\mu - z_B^\mu(\tau)), \quad (1)$$

where Q_A and Q_B are the internal degrees of freedom for the detectors Alice and Bob. They are assumed to be two identical harmonic oscillators with mass $m_0 = 1$ with the bare natural frequency Ω_0 [17].

If we assume that the coupling between the detectors and the field is turned on at the moment when $t = \tau = 0$ (t is the proper time for Alice and τ is the proper time for Bob), the state of this combined system is a direct product of a quantum state $|q_A, q_B\rangle$ for Alice's and Bob's detectors Q_A and Q_B and Minkowski vacuum $|0_M\rangle$ for the field Φ ,

$$|\psi(0)\rangle = |q_A, q_B\rangle \otimes |0_M\rangle. \quad (2)$$

Here $|q_A, q_B\rangle$ is taken to be a squeezed Gaussian state with minimal uncertainty, represented in the Wigner function as

$$\rho(Q_A, P_A, Q_B, P_B) = \exp - \frac{1}{8} \left[\frac{\beta^2}{\hbar^2} (Q_A + Q_B)^2 + \frac{1}{\alpha^2} (Q_A - Q_B)^2 + \frac{\alpha^2}{\hbar^2} (P_A - P_B)^2 + \frac{1}{\beta^2} (P_A + P_B)^2 \right], \quad (3)$$

where Q_A and Q_B can be entangled by properly choosing the parameters α and β .

After quantizing the field Φ and the internal degrees of freedom Q_A, Q_B in the Heisenberg picture (as shown in Appendix A), the mode functions to the first order $O(\lambda_0)$ for Φ, Q_A and Q_B are as follows:

$$(\partial_{\tau_i}^2 + \Omega_0^2) q_i^{(j)}(\tau_i) = \lambda_0 f^{(j)}(z_i^\mu(\tau_i)), \quad (4)$$

$$(\partial_t^2 - \nabla^2) f^{(j)}(x) = \lambda_0 \left[\int_0^\infty dt q_A^{(j)} \delta^4(x - z_A(t)) + \int_0^\infty d\tau q_B^{(j)} \delta^4(x - z_B(\tau)) \right], \quad (5)$$

$$(\partial_{\tau_i}^2 + \Omega_0^2) q_i^{(+)}(\tau_i, \mathbf{k}) = \lambda_0 f^{(+)}(z_i^\mu(\tau_i), \mathbf{k}), \quad (6)$$

$$(\partial_t^2 - \nabla^2) f^{(+)}(x, \mathbf{k}) = \lambda_0 \left[\int_0^\infty dt q_A^{(+)}(t, \mathbf{k}) \delta^4(x - z_A(t)) + \int_0^\infty d\tau q_B^{(+)}(\tau, \mathbf{k}) \delta^4(x - z_B(\tau)) \right]. \quad (7)$$

In future work, we would like to study issues pertaining to quantum teleportation after we obtain the solutions for \hat{Q}_A and \hat{Q}_B in this model. In this work, for simplicity and a clear picture, we will first look solely at the two-point functions of the internal degrees of freedom Q of the moving detector Bob. We will consider two different kinds of trajectories for Bob: (i) Bob is uniformly accelerated and (ii) Bob moves at a constant velocity. By calculating the solutions and the two-point correlation functions for Q of the detector Bob under these two types of trajectories, we will understand the features of acceleration and inertial motion and be able to apply these results to future applications.

III. TWO-POINT FUNCTIONS OF THE INTERNAL DEGREES OF FREEDOM Q FOR A MOVING DETECTOR

We now focus on the moving detector Bob. For simplicity, we consider only the moving detector Bob and temporarily ignore the static detector Alice in the action S in Eq. (1). The only action that has a Q_B part is then the following

$$S = - \int d^4x \sqrt{-g} \frac{1}{2} \partial_\mu \Phi(x) \partial^\mu \Phi(x) + \int d\tau_B \frac{m_0}{2} \left[(\partial_B Q_B)^2 - \Omega_0^2 Q_B^2 \right] + \lambda_0 \int d^4x \int d\tau_B Q_B(\tau_B) \Phi(x) \delta^4(x^\mu - z_B^\mu(\tau_B)). \quad (8)$$

The Heisenberg equations for the operators and the fields are written in [16] (we take $\hat{Q}_B = \hat{Q}$ from now on, and we also take $m_0 = 1$ in a later numerical calculation) are shown in Appendix B (including the solutions of the mode functions and the definitions of the states for the quantum field Φ and the internal degrees of freedom \hat{Q}). Later, we start with the two-point correlations function $\langle Q(\tau - \tau_0) Q(\tau'' - \tau_0'') \rangle_v$ for the moving detector Bob.

A. Trajectory 1: Two-point function for UAD

The two-point correlation function $\langle Q(\tau - \tau_0) Q(\tau'' - \tau_0'') \rangle_v$ of the internal degrees of freedom for the UAD Bob, which is along the trajectory $z_B^\mu = (a^{-1} \sinh a\tau, a^{-1} \cosh a\tau, 0, 0)$ with $a \neq 0$, is as follows:

$$\begin{aligned} & \langle Q(\tau - \tau_0) Q(\tau'' - \tau_0'') \rangle_v \\ &= \hbar \int_{-\infty}^{\infty} \frac{d^3k}{(2\pi)^3 2\omega} q^{(+)}(\tau; \mathbf{k}) q^{(-)}(\tau; \mathbf{k}) \\ &= \frac{\hbar}{2\omega} \int \frac{d^3\vec{k}}{(2\pi)^3} \frac{\lambda_0}{m_0} \sum_{j=+,-} \int_{\tau_0}^{\tau} d\tau' c_j e^{w_j(\tau-\tau')} f_0^{(+)}(z(\tau'), \vec{k}) \\ & \quad \cdot \frac{\lambda_0}{m_0} \sum_{j=+,-} \int_{\tau_0}^{\tau''} d\tau''' c_j^* e^{w_j^*(\tau''-\tau''')} f_0^{*(+)}(z(\tau'''), \vec{k}), \end{aligned} \quad (9)$$

The mode functions $q^{(\pm)}(\tau; \mathbf{k})$ for $\hat{Q}_v(\tau)$ [which are obtained in Eq. (61) in Appendix B] are

$$q^{(\pm)}(\tau; \mathbf{k}) = \frac{\lambda_0}{m_0} \sum_{j=+,-} \int_{\tau_0}^{\tau} d\tau' c_j e^{w_j(\tau-\tau')} f_0^{(\pm)}(z(\tau'); \mathbf{k}). \quad (10)$$

When a Fourier Transform of $f_0^{(+)}$ is performed,

$$f_0^{(+)}(z(\tau'), \vec{k}) = \int d\kappa e^{-i\kappa\tau'} \varphi_{\vec{k}}(\kappa), \quad (11)$$

the above two-point function is expressed as

$$\begin{aligned} & \langle Q(\tau - \tau_0) Q(\tau'' - \tau_0'') \rangle_v \\ &= \frac{\lambda_0^2}{m_0^2} \sum_{j,j'=+,-} \int_{\tau_0}^{\tau} d\tau' c_j e^{w_j(\tau-\tau')} \int d\kappa e^{-i\kappa\tau'} \int_{\tau_0''}^{\tau''} d\tau''' c_{j'}^* e^{w_{j'}(\tau''-\tau''')} \int d\kappa' e^{-i\kappa'\tau'''} \\ & \cdot F, \end{aligned} \quad (12)$$

where F is defined as

$$F \equiv \frac{\hbar}{2\omega} \int_{-\infty}^{\infty} \frac{d^3k}{2\pi} \varphi_{\vec{k}}(\kappa) \varphi_{\vec{k}}^*(\kappa'). \quad (13)$$

The Fourier factor $\varphi_{\vec{k}}(\kappa)$ is

$$\varphi_{\vec{k}}(\kappa) = \int_{-\infty}^{\infty} \frac{d\tau}{2\pi} e^{-i\omega z^0(\tau) + i\vec{k} \cdot \vec{z}(\tau)}, \quad (14)$$

and F is then in the following form:

$$\begin{aligned} F &= \frac{\hbar}{(2\pi)^3} \int_0^{2\pi} d\phi \int_{-1}^1 d(\cos\theta) \int_0^{\infty} \frac{\omega^2 d\omega}{2\omega} \int_{-\infty}^{+\infty} \frac{dt}{2\pi} \int_{-\infty}^{+\infty} \frac{dt'}{2\pi} e^{i\kappa t - i\kappa' t' - i\omega(z^0(t) - z^0(t') + i\omega \cos\theta |\vec{z} - \vec{z}'|)} \\ &= \frac{\hbar}{2\pi} \int_0^{\infty} d\omega \int_{-\infty}^{+\infty} \frac{dt}{2\pi} \int_{-\infty}^{+\infty} \frac{dt'}{2\pi} e^{i\kappa t - i\kappa' t' - i\omega[z^0(t) - z^0(t')]} \frac{\sin(\omega |\vec{z}(t) - \vec{z}(t')|)}{|\vec{z}(t) - \vec{z}(t')|} \\ &= \frac{\hbar}{(2\pi)^4} \lim_{\epsilon \rightarrow 0} \int_{-\infty}^{+\infty} dt \int_{-\infty}^{+\infty} dt' \frac{e^{i\kappa(t - \frac{i\epsilon}{2}) - i\kappa'(t' + \frac{i\epsilon}{2})}}{|\vec{z}(t - \frac{i\epsilon}{2}) - \vec{z}(t' + \frac{i\epsilon}{2})|^2 - [z^0(t - \frac{i\epsilon}{2}) - z^0(t' + \frac{i\epsilon}{2})]^2} \\ &= \frac{\hbar}{(2\pi)^4} \lim_{\epsilon \rightarrow 0} \int_{-\infty}^{+\infty} dt \int_{-\infty}^{+\infty} dt' \frac{a^2 e^{\frac{\epsilon}{2}(\kappa + \kappa') + i\kappa t - i\kappa' t'}}{-4 \sinh^2(\frac{a}{2}(t - t') - i\epsilon)} \\ &= \frac{\hbar}{(2\pi)^4} \lim_{\epsilon \rightarrow 0} \int_{-\infty}^{+\infty} dT \int_{-\infty}^{+\infty} d\Delta \frac{a^2 e^{\frac{\epsilon}{2}(\kappa + \kappa') + i(\kappa - \kappa')T + \frac{i\Delta}{2}(\kappa + \kappa')}}{-4 \sinh^2(\frac{a}{2}(\Delta - i\epsilon))} \\ &= \frac{\hbar a^2}{(2\pi)^3} \delta(\kappa - \kappa') \lim_{\epsilon \rightarrow 0} \int_{-\infty}^{+\infty} d\Delta \frac{e^{\kappa\epsilon} e^{i\kappa\Delta}}{-4 \sinh^2 \frac{a}{2}(\Delta - i\epsilon)}. \end{aligned} \quad (15)$$

On the third line of the equation, we take $t \rightarrow t - \frac{i\epsilon}{2}$ to suppress the contribution from high-frequency modes of the field, and this is equal to setting a finite time resolution of the system. On the fifth line of the equation, we take $T \equiv \frac{t+t'}{2}$ and $\Delta \equiv t - t'$, where the integral is the double complex integral. Note that there are poles at $\frac{a}{2}(\Delta - i\epsilon) = \pm i\bar{n}$ where $\bar{n} = 0, 1, 2, 3, \dots, \infty$. We then plug F back into the two-point function $\langle Q(\tau - \tau_0) Q(\tau'' - \tau_0'') \rangle_v$ and perform the integration of τ . Thus, we have the form

$$\langle Q(\tau - \tau_0) Q(\tau'' - \tau_0'') \rangle_v$$

$$\begin{aligned}
&= \frac{\lambda_0^2}{m_0^2} \sum_{j,j'=\pm} \int_{\tau_0}^{\tau} d\tau' c_j e^{w_j(\tau-\tau')} \int_{-\infty}^{+\infty} d\kappa e^{-i\kappa\tau'} \int_{\tau_0'}^{\tau''} d\tau''' c_{j'}^* e^{w_{j'}^*(\tau''-\tau''')} \int_{-\infty}^{+\infty} d\kappa' e^{i\kappa'\tau'''} \\
&\quad \cdot \frac{\hbar a^2}{(2\pi)^3} \delta(\kappa - \kappa') \lim_{\epsilon \rightarrow 0} \int_{-\infty}^{+\infty} d\Delta \frac{e^{\kappa\epsilon} e^{i\kappa\Delta}}{-4 \sinh^2 \frac{a}{2}(\Delta - i\epsilon)} \\
&= \frac{\lambda_0^2}{m_0^2} \frac{\hbar}{(2\pi)^2} \sum_{j,j'=\pm} \left(\frac{a^2}{2\pi} \lim_{\epsilon \rightarrow 0} \left[\int_0^{\infty} d\kappa e^{-i\kappa(\tau_0-\tau_0'')} \int_{-\infty}^{+\infty} d\Delta \frac{e^{\kappa\epsilon} e^{i\kappa\Delta}}{-4 \sinh^2 \frac{a}{2}(\Delta - i\epsilon)} \right. \right. \\
&\quad \left. \left. + \int_{-\infty}^0 d\kappa e^{-i\kappa(\tau_0-\tau_0'')} \int_{-\infty}^{+\infty} d\Delta \frac{e^{\kappa\epsilon} e^{i\kappa\Delta}}{-4 \sinh^2 \frac{a}{2}(\Delta + i\epsilon)} \right] \right) \\
&\quad \cdot \frac{c_j c_{j'}^* (e^{w_j(\tau-\tau_0)} - e^{i\kappa(\tau_0-\tau)}) (e^{w_{j'}^*(\tau''-\tau_0'')} - e^{i\kappa(\tau''-\tau_0'')})}{(w_j + i\kappa)(w_{j'}^* - i\kappa)}
\end{aligned} \tag{16}$$

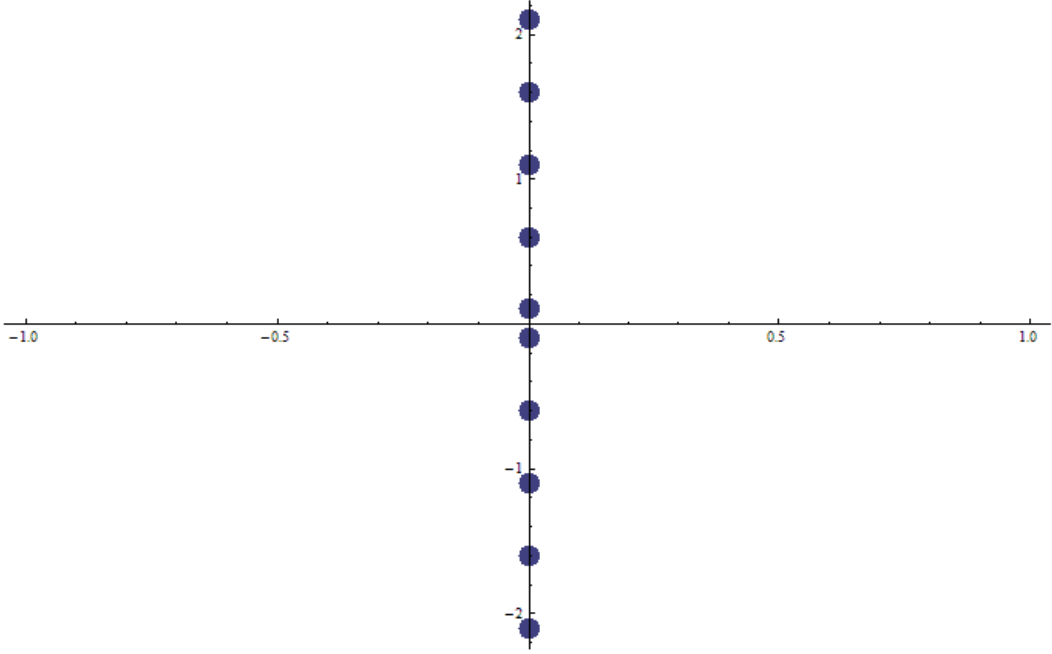


FIG. 1: Poles on the complex Δ plane at $\Delta = i(\epsilon + \frac{2\pi\bar{n}}{a})$ on the upper complex plane and at $\Delta = -i(\epsilon + \frac{2\pi\bar{n}}{a})$ on the lower complex plane. Where $\bar{n} = 0, 1, 2, 3, \dots, \infty$, the poles move to $\pm i\infty$ as $a \rightarrow 0$.

The integrals on the second equal sign in Eq.(16) are the tricky part (the double complex integrals). Note that inside the square brackets in Eq.(16), the κ and Δ double integrals are split into two parts because the sign of κ determines the contour integration is performed on the upper half complex plane or on the lower half plane. The first term in Eq.(17) is the Δ contour integral circle on the upper plane when $\kappa > 0$, while the second term Δ is the contour integral circle on the lower plane when $\kappa < 0$. The main different from previous result is that they did not separate the double complex integral and handle the part separately. If we did not notice this point, we would have just one term and would ignore the other term, as was done in the past.

For the double integrations, we have the following two parts:

$$\int_0^{\infty} d\kappa e^{-i\kappa(\tau'-\tau''')} \int_{-\infty}^{+\infty} d\Delta \frac{e^{\kappa\epsilon} e^{i\kappa\Delta}}{-4 \sinh^2 \frac{a}{2}(\Delta - i\epsilon)} + \int_{-\infty}^0 d\kappa e^{-i\kappa(\tau'-\tau''')} \int_{-\infty}^{+\infty} d\Delta \frac{e^{\kappa\epsilon} e^{i\kappa\Delta}}{-4 \sinh^2 \frac{a}{2}(\Delta + i\epsilon)}. \tag{17}$$

There are poles in the denominator $\sinh^2 \frac{a}{2}(\Delta - i\epsilon)$ at $\Delta = i(\epsilon + \frac{2\pi\bar{n}}{a})$ and poles in the other denominator $\sinh^2 \frac{a}{2}(\Delta + i\epsilon)$ at $\Delta = -i(\epsilon + \frac{2\pi\bar{n}}{a})$. We may use the identity

$$\csc^2 \pi x = \frac{1}{\pi^2} \sum_{n=-\infty}^{\infty} \frac{1}{(x-n)^2}, \quad (18)$$

and the relation $\sinh^2 x = -\sin^2(ix)$ to expand those poles.

We expand $\sinh x$ in the first integral such that

$$\frac{-1}{4 \sinh^2 \frac{a}{2}(\Delta - i\epsilon)} = \frac{1}{4 \sin^2(\frac{ia\Delta}{2} + \epsilon)} = \frac{-1}{a^2} \sum_{n=-\infty}^{\infty} \frac{1}{(\Delta - i\epsilon + i2\pi n/a)^2}. \quad (19)$$

In the first integral of Eq. (17), only the poles $n = 0, -1, -2, \dots, -\infty$ are inside the contour. Let $\bar{n} = -n$ in the first integral and rewrite it in the following way:

$$\begin{aligned} & \int_0^{\infty} d\kappa e^{-i\kappa(\tau' - \tau''')} \int_{-\infty}^{+\infty} d\Delta \frac{e^{\kappa\epsilon} e^{i\kappa\Delta}}{-4 \sinh^2 \frac{a}{2}(\Delta - i\epsilon)} \\ &= \int_0^{\infty} d\kappa e^{-i\kappa(\tau' - \tau''')} \int_{-\infty}^{+\infty} d\Delta \sum_{\bar{n}=0}^{\infty} \frac{e^{\kappa\epsilon} e^{i\kappa\Delta}}{-a^2 [\Delta - i(\epsilon + 2\pi\bar{n}/a)]^2}, \end{aligned} \quad (20)$$

where the given terms 2π and n are absorbed into ϵ . Similarly, the second integral in Eq.(17) is expanded in the same way:

$$\frac{-1}{4 \sinh^2 \frac{a}{2}(\Delta + i\epsilon)} = \frac{1}{4 \sin^2(\frac{ia\Delta}{2} - \epsilon)} = \frac{-1}{a^2} \sum_{n=-\infty}^{\infty} \frac{1}{(\Delta + i\epsilon + i2\pi n/a)^2}. \quad (21)$$

Only the poles $n = 0, 1, 2, \dots, \infty$ are inside the contour of the second integral. Therefore, the second integral is rewritten as

$$\begin{aligned} & \int_{-\infty}^0 d\kappa e^{-i\kappa(\tau' - \tau''')} \int_{-\infty}^{+\infty} d\Delta \frac{e^{\kappa\epsilon} e^{i\kappa\Delta}}{-4 \sinh^2 \frac{a}{2}(\Delta + i\epsilon)} \\ &= \int_{-\infty}^0 d\kappa e^{-i\kappa(\tau' - \tau''')} \int_{-\infty}^{+\infty} d\Delta \sum_{n=0}^{\infty} \frac{e^{\kappa\epsilon} e^{i\kappa\Delta}}{-a^2 [\Delta + i(\epsilon + 2\pi n/a)]^2}, \end{aligned} \quad (22)$$

In our spacetime diagram $a \leq 1$ (we assume the light speed $c = 1$, so the proper acceleration $a \leq 1$). Note that when $a \rightarrow 0$ the poles on the complex Δ plane move to ∞ and the arc integration $\int_{arc} d\Delta f(\Delta)$ in Cauchy's integral formula is no longer 0 (the arc cannot include the poles when the poles move to ∞); the integral is ill defined. And if we think carefully, back to Fig. 2 and check the worldline for the detector Bob, we can see that as $a \rightarrow 0$, Bob is very far from origin, and thus Bob cannot exchange the signal with Alice in a finite time interval. This situation is not the setup that we want (we need Alice and Bob to be separated by a proper distance so that they can exchange signals with each other in a reasonable time interval and we can study the properties in the quantum teleportation process in such a setup in the future work). Therefore, the result when $a \rightarrow 0$ in Eq. (17) is not the actual setup that can be extended to the case in which Alice and Bob have a finite distance between them and exchange signals when Bob moves at a constant velocity.

Plugging Eq.(20) and (22) back into Eq.(16), we have

$$\frac{-1}{a^2} \lim_{\epsilon \rightarrow 0} \left(\int_0^{\infty} d\kappa \int_{-\infty}^{\infty} d\Delta \sum_{\bar{n}=0}^{\infty} \frac{e^{\kappa\epsilon} e^{i\kappa\Delta}}{[\Delta - i(\epsilon + \frac{2\pi\bar{n}}{a})]^2} + \int_{-\infty}^0 d\kappa \int_{-\infty}^{\infty} d\Delta \sum_{\bar{n}=0}^{\infty} \frac{e^{\kappa\epsilon} e^{i\kappa\Delta}}{[\Delta + i(\epsilon + \frac{2\pi\bar{n}}{a})]^2} \right), \quad (23)$$

Performing the Δ integration (taking $\epsilon = 0$ in the end), we then have the following

$$\begin{aligned} & \frac{-1}{a^2} \left(\int_0^{\infty} d\kappa \sum_{\bar{n}=0}^{\infty} (2\pi i) i\kappa e^{i\kappa i(\frac{2\pi\bar{n}}{a})} + \int_{-\infty}^0 d\kappa \sum_{\bar{n}=0}^{\infty} (-2\pi i) i\kappa e^{i\kappa i(-\frac{2\pi\bar{n}}{a})} \right) \\ &= \frac{-1}{a^2} \left(\int_0^{\infty} d\kappa \sum_{\bar{n}=0}^{\infty} (2\pi i) i\kappa e^{i\kappa i(\frac{2\pi\bar{n}}{a})} - \int_{-\infty}^0 d\kappa \sum_{\bar{n}=0}^{\infty} (2\pi i) i\kappa e^{-i\kappa i(\frac{2\pi\bar{n}}{a})} \right). \end{aligned} \quad (24)$$

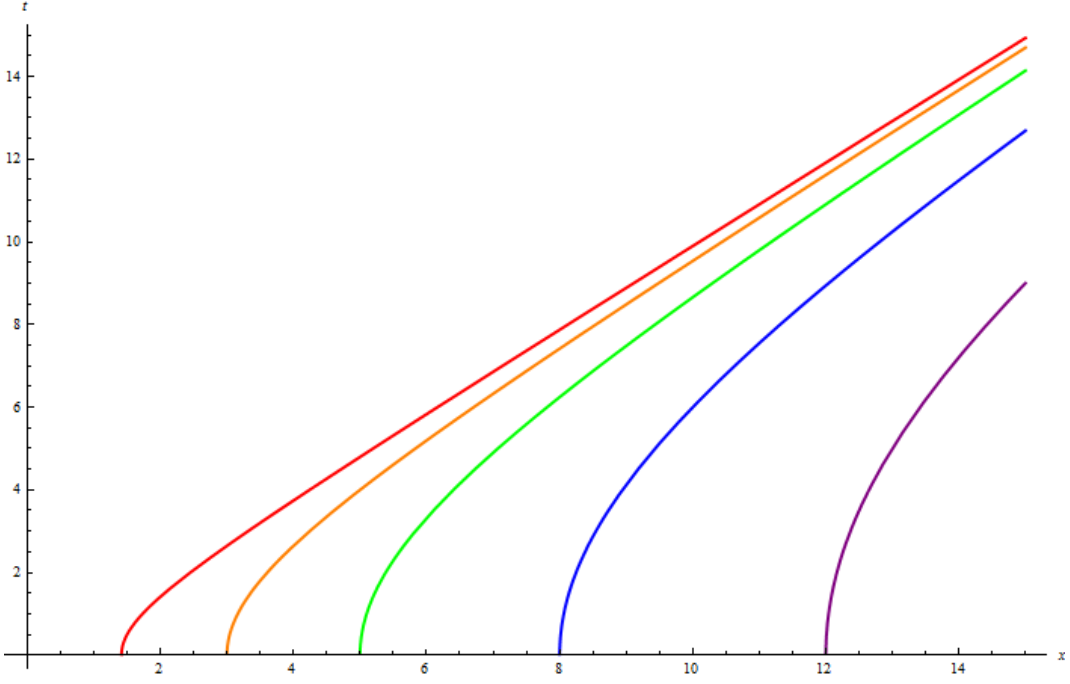


FIG. 2: The plot of the worldline $z_B^\mu = (a^{-1} \sinh a\tau, a^{-1} \cosh a\tau, 0, 0)$ for differing proper acceleration values a . As the proper acceleration $a \rightarrow 0$, the worldline is shifted far away. The proper acceleration of the red line is the largest among all lines, while the proper acceleration of the purple line is the smallest among all lines.

Plugging the above result back into Eq. (16), we obtain the following terms:

$$\begin{aligned}
& \frac{-1}{a^2} \left(\int_0^\infty d\kappa \sum_{\bar{n}=0}^\infty (2\pi i) i\kappa e^{i\kappa i(\frac{2\pi\bar{n}}{a})} - \int_{-\infty}^0 d\kappa \sum_{\bar{n}=0}^\infty (2\pi i) i\kappa e^{-i\kappa i(\frac{2\pi\bar{n}}{a})} \right) e^{-i\kappa(\tau_0 - \tau_0'')} \\
& \frac{C_j C_{j'}^* (e^{w_j(\tau - \tau_0)} - e^{i\kappa(\tau_0 - \tau)}) (e^{w_{j'}^*(\tau'' - \tau_0'')} - e^{i\kappa(\tau'' - \tau_0'')})}{(w_j + i\kappa)(w_{j'}^* - i\kappa)} \\
& = \frac{-1}{a^2} \left[\int_0^\infty d\kappa \sum_{\bar{n}=0}^\infty X^{\bar{n}} F(\kappa) - \int_{-\infty}^0 d\kappa \sum_{\bar{n}=0}^\infty X^{-\bar{n}} F(\kappa) \right], \tag{25}
\end{aligned}$$

where $X^{\bar{n}} = e^{-\kappa \frac{2\pi}{a}}$ and $F(\kappa) = (2\pi i) i\kappa \cdot \frac{C_j C_{j'}^* (e^{w_j(\tau - \tau_0)} - e^{i\kappa(\tau_0 - \tau)}) (e^{w_{j'}^*(\tau'' - \tau_0'')} - e^{i\kappa(\tau'' - \tau_0'')}) e^{-i\kappa(\tau_0 - \tau_0'')}}{(w_j + i\kappa)(w_{j'}^* - i\kappa)}$.

Note that since there are many poles on the imaginary axis of the κ complex plane, it is difficult to do a contour integration in the form of Eq.(25). To avoid the difficulty of such contour integral, we can reshape Eq. (25) in the following way to avoid the poles:

$$\begin{aligned}
& \frac{-1}{a^2} \left[\int_0^\infty d\kappa \sum_{\bar{n}=0}^\infty X^{\bar{n}} - \int_{-\infty}^0 d\kappa \sum_{\bar{n}=0}^\infty X^{-\bar{n}} \right] F(\kappa) \\
& = \frac{-1}{a^2} \left[\int_0^\infty d\kappa \frac{1}{1-X} - \int_{-\infty}^0 d\kappa \frac{1}{1-X^{-1}} \right] F(\kappa) \\
& = \frac{-1}{a^2} \left[\int_0^\infty d\kappa \frac{1}{1-X} - \int_{-\infty}^0 d\kappa \frac{X}{X-1} \right] F(\kappa) \\
& = \frac{-1}{a^2} \left[\int_0^\infty d\kappa \frac{1}{1-X} + \int_{-\infty}^0 d\kappa \frac{X-1+1}{1-X} \right] F(\kappa) \\
& = \frac{-1}{a^2} \left[\int_0^\infty d\kappa \frac{1}{1-X} + \int_{-\infty}^0 d\kappa \frac{1}{1-X} + \int_{-\infty}^0 d\kappa \frac{X-1}{1-X} \right] F(\kappa)
\end{aligned}$$

$$= \frac{-1}{a^2} \left[\int_{-\infty}^{\infty} \frac{d\kappa F(\kappa)}{1-X} - \int_{-\infty}^0 d\kappa F(\kappa) \right]. \quad (26)$$

When we use the above trick (we rewrite the integral region from $-\infty$ to ∞ and include the poles inside the contour in the first integral), the difficult contour integral from 0 to ∞ is prevented.

We then put the above results back into Eq. (16), and then the two-point function in Eq. (16) is thus reshaped as

$$\begin{aligned} & \langle Q(\tau - \tau_0)Q(\tau'' - \tau_0'') \rangle_v \\ &= \frac{\lambda_0^2 \hbar}{m_0^2 (2\pi)^2} \left[\sum_{j,j'=\pm} C_j C_{j'}^* \int_{-\infty}^{\infty} \frac{\kappa d\kappa e^{-i\kappa(\tau_0 - \tau_0'')} (e^{w_j(\tau - \tau_0)} - e^{i\kappa(\tau_0 - \tau)}) (e^{w_{j'}^*(\tau'' - \tau_0'')} - e^{i\kappa(\tau'' - \tau_0'')})}{(1 - e^{-2\pi\kappa/a})(w_j + i\kappa)(w_{j'}^* - i\kappa)} \right. \\ & \quad \left. - \sum_{j,j'=\pm} C_j C_{j'}^* \int_{-\infty}^0 \frac{\kappa d\kappa e^{-i\kappa(\tau_0 - \tau_0'')} (e^{w_j(\tau - \tau_0)} - e^{i\kappa(\tau_0 - \tau)}) (e^{w_{j'}^*(\tau'' - \tau_0'')} - e^{i\kappa(\tau'' - \tau_0'')})}{(w_j + i\kappa)(w_{j'}^* - i\kappa)} \right], \quad (27) \end{aligned}$$

and we have two terms in the two-point correlation function. Note that the first term is the old result in the previous work, while the second term is the new result that is missing from the previous work.

The steps above are the key points in the calculations. To avoid the difficult κ integration (many poles on the imaginary axis of the κ plane) we thus reshape Eq. (16) into the form of Eq. (27). When we compare this new result to the previous result, we find that the second term in Eq. (27) is missing from the previous results. This is a careless accident that can happen when we deal with the double complex integral in Eq. (16). Also, remember that when $a = 0$ the result of this two-point function is no longer true, because this result corresponds to the situation in which Bob is very far away, so Bob and Alice cannot exchange messages within a reasonable time interval. The mathematical reason for this is shown in the part of Δ contour integration, where the denominator $\sinh^2 \frac{a}{2}(\Delta - i\epsilon)$ of the Δ integration on the last line of Eq. (16) is no longer a hyperbolic sine function as $a = 0$. This corresponds to Fig. 2, in which the world line of Bob shifts to very far away as $a = 0$, and this is not the setup that we want.

If we compare the difference of this new result for the two-point correlation function more easily to the previous one [16]), the two-point correlation function is expressed in the following form:

$$\begin{aligned} & \langle Q(\tau - \tau_0)Q(\tau'' - \tau_0'') \rangle_v \\ &= \frac{\lambda_0^2 \hbar}{(2\pi)^2 m_0^2} \sum_{j,j'} \int_0^{\infty} \frac{\kappa d\kappa}{1 - e^{-2\pi\kappa/a}} \frac{C_j C_{j'}^* e^{-i\kappa(\tau_0 - \tau_0'')}}{(w_j + i\kappa)(w_{j'}^* - i\kappa)} (e^{w_j(\tau - \tau_0)} - e^{-i\kappa(\tau - \tau_0)}) (e^{w_{j'}^*(\tau'' - \tau_0'')} - e^{i\kappa(\tau'' - \tau_0'')}) \\ &= \frac{\lambda_0^2 \hbar}{m_0^2 (2\pi)^2} \left[\sum_{j,j'=\pm} C_j C_{j'}^* \int_{-\infty}^{\infty} \frac{\kappa d\kappa e^{-i\kappa(\tau_0 - \tau_0'')} (e^{w_j(\tau - \tau_0)} - e^{i\kappa(\tau_0 - \tau)}) (e^{w_{j'}^*(\tau'' - \tau_0'')} - e^{i\kappa(\tau'' - \tau_0'')})}{(1 - e^{-2\pi\kappa/a})(w_j + i\kappa)(w_{j'}^* - i\kappa)} \right. \\ & \quad \left. - \sum_{j,j'=\pm} C_j C_{j'}^* \int_{-\infty}^0 \frac{\kappa d\kappa e^{-i\kappa(\tau_0 - \tau_0'')} (e^{w_j(\tau - \tau_0)} - e^{i\kappa(\tau_0 - \tau)}) (e^{w_{j'}^*(\tau'' - \tau_0'')} - e^{i\kappa(\tau'' - \tau_0'')})}{(w_j + i\kappa)(w_{j'}^* - i\kappa)} \right] \\ &= \langle QQ \rangle_{v1} - \langle QQ \rangle_{v2}. \quad (28) \end{aligned}$$

The first term $\langle QQ \rangle_{v1}$ is the old result from the previous work([16]), and the second term $\langle QQ \rangle_{v2}$ is the missing term(a new term). The advantage of the two-point function being reshaped in the above manner is that it can be compared and computed more easily since the poles on the imaginary axis are now included inside the contour and the κ integrations can be done. Also, we can easily compare this new result to the old result([16]) and see the differences between the new and old results more clearly.

Here we simply write the results of $\langle QQ \rangle_{v1}$, and $-\langle QQ \rangle_{v2}$ in Eq. (28) below, the detailed derivations is written in Appendix D.

$$\begin{aligned} & \langle QQ \rangle_{v1} \\ &= \frac{2\hbar\gamma}{\pi m_0 \Omega^2} \theta(\eta) \text{Re}\{(\Lambda_0 - \ln \frac{a}{\Omega}) e^{-2\gamma\eta} \sin^2 \Omega\eta\} \\ & \quad + \frac{a}{2} e^{-(\gamma+a)\eta} \left[\frac{F_{\gamma+i\Omega}(e^{-a\eta})}{\gamma+i\Omega+a} \left(\frac{-i\Omega}{\gamma} \right) e^{-i\Omega\eta} + \frac{F_{-\gamma-i\Omega}(e^{-a\eta})}{\gamma+i\Omega-a} \left(\left(1 + \frac{i\Omega}{\gamma} \right) e^{i\Omega\eta} - e^{-i\Omega\eta} \right) \right] \end{aligned}$$

$$\begin{aligned}
& -\frac{1}{4} \left[\left(\frac{i\Omega}{\gamma} + e^{-2\gamma\eta} \left(\frac{i\Omega}{\gamma} + 1 - e^{-2i\Omega\eta} \right) \right) (\psi_{\gamma+i\Omega} + \psi_{-\gamma-i\Omega}) \right. \\
& \quad \left. - \left(\frac{-i\Omega}{\gamma} + e^{-2\gamma\eta} \left(\frac{i\Omega}{\gamma} + 1 - e^{-2i\Omega\eta} \right) \right) i\pi \coth \frac{\pi}{a} (\Omega - i\gamma) \right] \}. \tag{29}
\end{aligned}$$

$$\begin{aligned}
& -\langle QQ \rangle_{v2} \\
& = \frac{-2\hbar\gamma}{\pi m_0} Re \left\{ \Lambda_{0,v2} - \frac{e^{-2\gamma(\tau-\tau_0)}}{8\Omega^2} \left[\left(1 - \frac{i\Omega}{\gamma} - e^{2i\Omega(\tau-\tau_0)} \right) \cdot (i\pi + 2 \log(\gamma - i\Omega) + 2\Gamma(0, -(\gamma - i\Omega)(\tau - \tau_0))) \right. \right. \\
& \quad \left. \left. + \left(1 + \frac{i\Omega}{\gamma} - e^{-2i\Omega(\tau-\tau_0)} \right) \cdot (-i\pi - 2 \log(\gamma + i\Omega) + 2\Gamma(0, -(\gamma + i\Omega)(\tau - \tau_0))) \right] \right\} \\
& \quad - \frac{i}{8\Omega\gamma} \left[-i\pi - 2 \log\left(\frac{\gamma + i\Omega}{\gamma - i\Omega}\right) + 2\Gamma(0, (\gamma + i\Omega)(\tau - \tau_0)) - 2\Gamma(0, (\gamma - i\Omega)(\tau - \tau_0)) \right] \}, \tag{30}
\end{aligned}$$

where Λ_0 and $\Lambda_{0,v2}$ are the terms containing the divergent parts $[\Gamma(0,0)$ and $\log(0)]$ as $\tau'' \rightarrow \tau$ and $\tau_0'' \rightarrow \tau_0$, and are absorbed into the renormalized constant or coefficient in the experiment. Figure 3- 5 are the numerical results for $\langle QQ \rangle_{v1}$ and $-\langle QQ \rangle_{v2}$. In the plots, the red line is the term $\langle QQ \rangle_{v1}$ (i.e., the old result) and the blue line is the term $-\langle QQ \rangle_{v2}$ (i.e., the missing term), while the black line is the sum $\langle QQ \rangle_{v1} - \langle QQ \rangle_{v2}$. The contributions from the vacuum fluctuations of the two-point function $\langle QQ \rangle_v$ (i.e., the black line) for the internal degrees of freedom Q begin with a relatively high value, then oscillate and reach to a saturated value at a later time.

In fig. 3, we change the proper acceleration a and keep the other parameters the same. We can see that for $a = 0.1$ and $a = 0.001$, the black curves have the same shape, but the values are slightly different. The value of the two-point function $\langle QQ \rangle_v$ for the $a = 0.1$ curve is just higher than the $a = 0.001$ curve for only a very small number, 0.00001. If we think that a uniformly accelerated detector would experience a different thermal radiance-a different temperature in the background(the Unruh effect)-this different background would produce different vacuum fluctuations for $\langle QQ \rangle_v$. Thus, we can see that although the difference of the effect from proper acceleration from $a = 0.1$ to $a = 0.001$ UAD is small, it is indeed present.

In Fig. 4, we change the value of the coupling constant λ_0 , or, say we change the decay parameter γ . This is because the definition $\gamma = \frac{\lambda_0^2}{8\pi m_0}$ and we also use perturbations method in these computations. Therefore, $\lambda_0 < 1$ is the basic assumption for perturbation (i.e., λ_0 is the expansion parameter). The allowed region for γ is then $\gamma < 0.039$. In the previous work[16], we chose $\gamma = 0.1$, which is equal to $\lambda_0 = 1.585$. This value is too big and obviously violates the basic assumption of the perturbation, making the perturbative solutions inconsistent with the perturbation method. According to our experience, a safe choice is to make the expansion parameter $\lambda_0 \approx 0.1$. This is why we choose $\lambda_0 = 0.1$ and 0.3(corresponding to $\gamma = 0.000398$ and 0.00358) in our numerical plots.

In Fig. 5, we alter the value of frequency Ω (i.e., the frequency for the internal degrees of freedom of the detector) and keep the other parameters the same. We choose $\Omega = 2.3$ and 1.0, and the magnitude of the two-point function $\langle QQ \rangle_v$ for $\Omega = 2.3$ is larger than in the $\Omega = 1.0$ case. Also, in the same τ interval, the curve for the $\Omega = 2.3$ case has more oscillations than the curve for the $\Omega = 1.0$ case does.

As in the calculations of the two-point function $\langle QQ \rangle$, we also compute the two-point function $\langle \dot{Q}\dot{Q} \rangle$, and the result is listed below. As shown above, there is an extra term $-\langle \dot{Q}\dot{Q} \rangle_{v2}$ in our new result which is missing from the previous result [16].

$$\begin{aligned}
& \langle \dot{Q}\dot{Q} \rangle_{v1} \\
& = \frac{2\hbar\gamma}{\pi m_0 \Omega^2} \theta(\eta) Re \left\{ (\Lambda_1 - \ln \frac{a}{\Omega}) \Omega^2 + (\Lambda_0 - \ln \frac{a}{\Omega}) e^{-2\gamma\eta} (\Omega \cos \Omega\eta - \gamma \sin \Omega\eta)^2 \right. \\
& \quad \left. + \frac{a}{2} (\gamma + i\Omega)^2 e^{-(\gamma+a)\eta} \left[\frac{F_{\gamma+i\Omega}(e^{-a\eta})}{\gamma + i\Omega + a} \left(\frac{i\Omega}{\gamma} \right) e^{-i\Omega\eta} + \frac{F_{-\gamma-i\Omega}(e^{-a\eta})}{\gamma + i\Omega - a} \left(\left(1 - \frac{i\Omega}{\gamma} \right) e^{i\Omega\eta} - e^{-i\Omega\eta} \right) \right] \right\} \\
& \quad + \frac{1}{4} (\gamma + i\Omega)^2 \left[\left(\frac{i\Omega}{\gamma} + e^{-2\gamma\eta} \left(\frac{i\Omega}{\gamma} - 1 + e^{-2i\Omega\eta} \right) \right) (\psi_{\gamma+i\Omega} + \psi_{-\gamma-i\Omega}) \right. \\
& \quad \left. - \left(\frac{-i\Omega}{\gamma} + e^{-2\gamma\eta} \left(\frac{i\Omega}{\gamma} - 1 + e^{-2i\Omega\eta} \right) \right) i\pi \coth \frac{\pi}{a} (\Omega - i\gamma) \right] \}. \tag{31}
\end{aligned}$$

$$\begin{aligned}
& -\langle \dot{Q}\dot{Q} \rangle_{v2} \\
= & \frac{-2\hbar\gamma}{\pi m_0} \theta(\eta) \text{Re} \{ \tilde{\Lambda}_{0v2} + \frac{e^{-2\gamma(\tau-\tau_0)}}{8\Omega^2} \left[((\gamma^2 + \Omega^2)(1 - \frac{i\Omega}{\gamma}) - (\gamma - i\Omega)^2 e^{2i\Omega(\tau-\tau_0)}) \right. \\
& \cdot (-i\pi + 2 \log(\gamma - i\Omega)) + ((\gamma^2 + \Omega^2)(1 + \frac{i\Omega}{\gamma}) - (\gamma + i\Omega)^2 e^{-2i\Omega(\tau-\tau_0)}) \cdot (i\pi + 2 \log(\gamma + i\Omega)) \left. \right] \\
& + \frac{ie^{-(\gamma+i\Omega)(\tau-\tau_0)}}{4\Omega\gamma} \left[(\gamma - i\Omega) \left(\frac{-1}{\tau - \tau_0} + e^{(\gamma-i\Omega)(\tau-\tau_0)} (\gamma - i\Omega) \Gamma(0, (\gamma - i\Omega)(\tau - \tau_0)) \right) - (\gamma + i\Omega) \right. \\
& \cdot \left. \left(\frac{-1}{\tau - \tau_0} + e^{(\gamma+i\Omega)(\tau-\tau_0)} (\gamma + i\Omega) \Gamma(0, (\gamma + i\Omega)(\tau - \tau_0)) \right) \right] \\
& + \frac{e^{-\gamma(\tau-\tau_0)}}{4\Omega^2} \left[((\gamma + i\Omega)e^{-i\Omega(\tau-\tau_0)} - \frac{\gamma^2 + \Omega^2}{\gamma} e^{i\Omega(\tau-\tau_0)}) ((\gamma + i\Omega)(i\pi - \Gamma(0, -(\gamma + i\Omega)(\tau - \tau_0))) \right. \\
& \cdot e^{-(\gamma+i\Omega)(\tau-\tau_0)} - \frac{1}{\tau - \tau_0}) + ((\gamma - i\Omega)e^{i\Omega(\tau-\tau_0)} - \frac{\gamma^2 + \Omega^2}{\gamma} e^{-i\Omega(\tau-\tau_0)}) \cdot (e^{(-\gamma+i\Omega)(\tau-\tau_0)}(-\gamma + i\Omega) \\
& \cdot (i\pi + \Gamma(0, (-\gamma + i\Omega)(\tau - \tau_0))) - \frac{1}{\tau - \tau_0}) \left. \right] + \frac{i}{8\Omega\gamma} [(\gamma - i\Omega)^2 (2 \log(\gamma - i\Omega) + i\pi) \\
& - (\gamma + i\Omega)^2 (2 \log(\gamma + i\Omega) + 3i\pi)] \}, \tag{32}
\end{aligned}$$

where Λ_1 , Λ_0 , and $\tilde{\Lambda}_{0v2}$ are the terms contains those divergent parts $\Gamma(0, 0)$ and $\log(0)$ as $\tau'' \rightarrow \tau$ and $\tau_0'' \rightarrow \tau_0$, and they are absorbed into the renormalized constant or coefficient in the experiment.

The above numerical results are plotted in the following Figs. 6- 8. The red line is the term $\langle \dot{Q}\dot{Q} \rangle_{v1}$, while the green line is the missing term $-\langle \dot{Q}\dot{Q} \rangle_{v2}$ and the black line is the sum $\langle \dot{Q}\dot{Q} \rangle_{v1} - \langle \dot{Q}\dot{Q} \rangle_{v2}$.

In Fig 6, we vary the value a and find the magnitude of $\langle \dot{Q}\dot{Q} \rangle_v$ for different a ($a = 0.1$ or 0.001) at the same time that τ is unchanged. The effect of the proper acceleration a is not obvious. The curve at first is arising slightly and then decreasing and oscillating. The trend for $\langle \dot{Q}\dot{Q} \rangle_v$ is decreasing and different from $\langle QQ \rangle_v$, which is slightly increasing.

In Fig. 7, we vary the decay parameter γ (which is equivalent to varying the coupling constant λ_0). The curve for the two-point function $\langle \dot{Q}\dot{Q} \rangle_v$ also rises slightly in the beginning and then oscillates and decreases to a saturated value. The difference is that the curve for $\gamma = 0.00358$ arrives at the saturated value earlier than $\gamma = 0.000398$. At the same time τ , the value of the two-point function $\langle \dot{Q}\dot{Q} \rangle_v$ for different γ is also slightly different. The reason for this is that a higher γ value for the two-point function curve decays to the same value faster than a lower γ curve does.

In Fig. 8, we alter the frequency of the internal degrees of freedom for the detector. It is obvious that the magnitude of $\langle \dot{Q}\dot{Q} \rangle_v$ changes significantly when the internal frequency Ω is altered. The trend of both curves is the same in that at first it has a small rise and then it decays and oscillates to a saturated value. However, a large Ω has more oscillations in its decay curve. A small Ω is less active than a large Ω . And also, a small Ω curve has a much lower saturated value than a large Ω curve.

The red lines in the plots represent the old results for the two-point functions $\langle \dot{Q}\dot{Q} \rangle_v$ which are displayed as a dotted line in Fig. 2 of Ref. [16]. The old results do not have the missing term $-\langle \dot{Q}\dot{Q} \rangle_{v2}$ (the green line). The black line is the sum $\langle \dot{Q}\dot{Q} \rangle_{v1} - \langle \dot{Q}\dot{Q} \rangle_{v2}$, and it gradually drops to a steady value at late time. This differs from the old result. The two-point functions $\langle \dot{Q}\dot{Q} \rangle_v$ in the old result increase gradually to a steady value.

Comparing the above plots for the two-point function $\langle \dot{Q}\dot{Q} \rangle_v$ to the plots for the two-point function $\langle QQ \rangle_v$, we find that the difference between $\langle QQ \rangle_v$ and $\langle \dot{Q}\dot{Q} \rangle_v$ is that the proper acceleration parameter a affects the trend of the oscillating curve in the early-time region (whether it is slightly increasing or decreasing). The coupling constant λ_0 affects how soon the curve of $\langle \dot{Q}\dot{Q} \rangle_v$ arrives at the saturated value as shown in Fig. 7. The frequency Ω affects how large the final saturated value for $\langle \dot{Q}\dot{Q} \rangle_v$ will be. As shown in Fig. 8, a smaller Ω has a smaller saturated value.

Next, we will discuss the allowed region for the value of the coupling constant λ_0 , which is about the decay constant γ . This part was not noticed before.

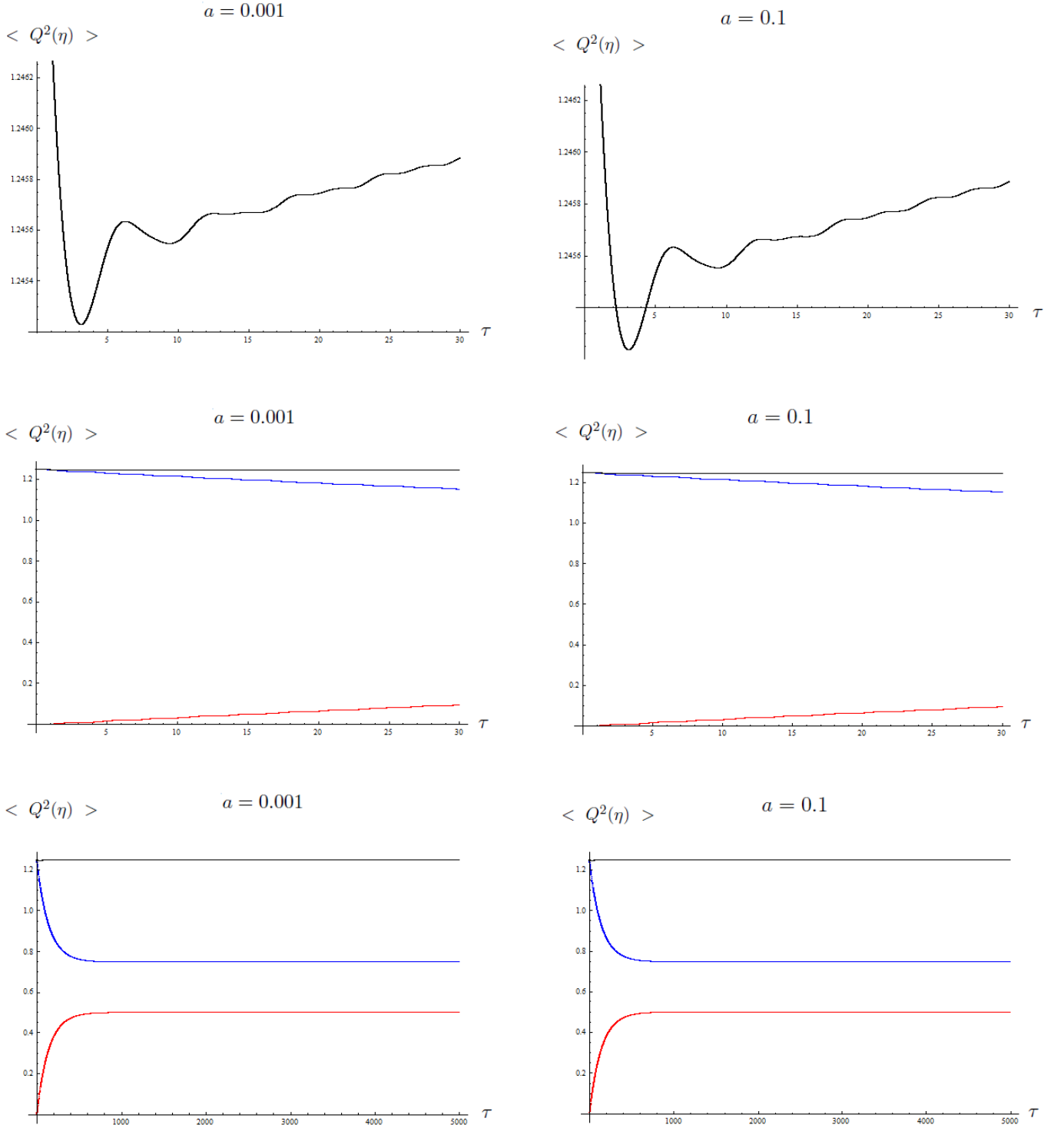


FIG. 3: The plots for $\langle Q^2(\eta) \rangle_{v1}$ [red line; Eq. (29) with Λ_0 excluded], $-\langle Q^2(\eta) \rangle_{v2}$ [blue line; Eq. (30) with $\Lambda_{0,v2}$ excluded], and the sum $\langle Q^2(\eta) \rangle_v$ [i.e., black line $\langle Q^2(\eta) \rangle_{v1} - \langle Q^2(\eta) \rangle_{v2}$]. Here $\Omega = 1.0$, $\lambda_0 = 0.3$ (which is $\gamma = 0.00358$), and $m_0 = \hbar = 1$. Note that $-\langle Q^2(\eta) \rangle_{v2}$ is larger than $\langle Q^2(\eta) \rangle_{v1}$. The black line [i.e., $\langle Q^2(\eta) \rangle_v$] oscillates at the beginning and arrives at the saturated value later. When $t = 30$, the curve for the proper acceleration $a = 0.1$ arrives at the value 1.24589, while the curve for a smaller proper acceleration $a = 0.001$ arrives at the value 1.24588; the difference is only 0.00001. When $t = 5000$, curves for both small or large proper acceleration values arrive at the same final magnitude 1.24772.

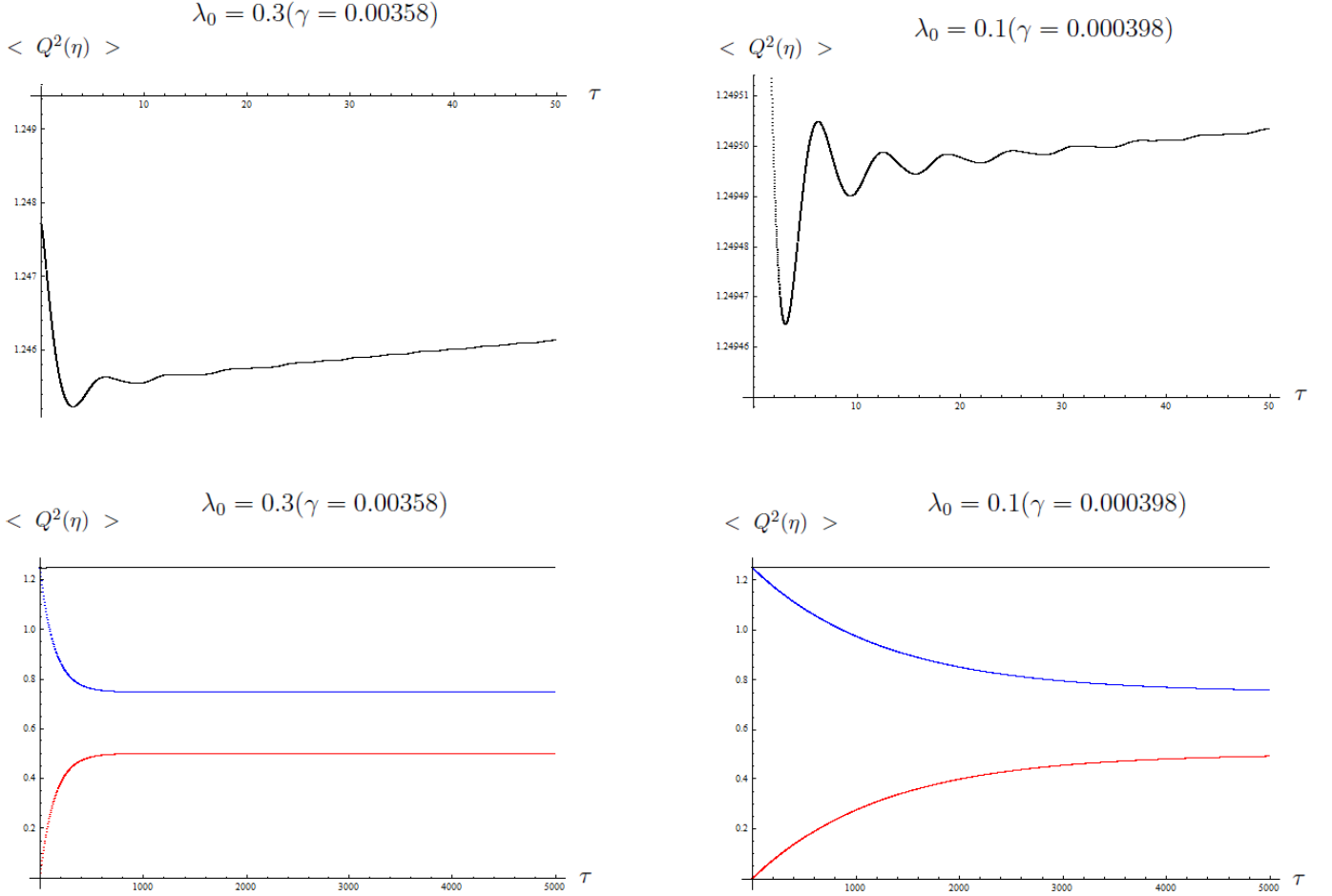


FIG. 4: The decay parameter $\gamma (\gamma = \frac{\lambda_0^2}{8\pi m_0})$. The plots for $\langle Q^2(\eta) \rangle_{v1}$ [red line; Eq. (29) with Λ_0 excluded], $-\langle Q^2(\eta) \rangle_{v2}$ [blue line; Eq. (30) with Λ_{0v2} excluded], and the sum $\langle Q^2(\eta) \rangle_v$ [black line, which is $\langle Q^2(\eta) \rangle_{v1} - \langle Q^2(\eta) \rangle_{v2}$]. Here $\Omega = 1.0$, $a = 0.001$, and $m_0 = \hbar = 1$. The decay parameters are different in the plots. The black lines oscillate at the beginning and then arrive at different saturated values later at proper time $\tau = 5000$ for different λ_0 . When $\tau = 50$, the final value for $\gamma = 0.000398$ is 1.2495, while when $\tau = 50$ the final value for $\gamma = 0.00358$ is 1.24613. When $\tau = 5000$, the final value for $\gamma = 0.000398$ is 1.24974, while when $\tau = 5000$ the final value for $\gamma = 0.00358$ is 1.24772. A large $\lambda_0 (\lambda_0 = 0.3)$ has a larger value than a smaller $\lambda_0 (\lambda_0 = 0.1)$, while a smaller λ_0 arrives at the same saturated value later than a larger $\lambda_0 (\lambda_0 = 0.3)$. The decay parameter γ affects the saturated time.

B. Allowed region for γ : Proper and improper value for γ concerning the contribution of the missing term $-\langle QQ \rangle_{v2}$

The γ value has some restrictions. In Sec.II Appendix B, we expand the mode function $f^{(\pm)}$ and $q^{(\pm)}$ by the order of λ_0 , then use the perturbative method to obtain the leading order solutions for $q^{(\pm)}$. Later, we use the leading order solution to compute $\langle Q^2(\eta) \rangle_v$ to the first order $O(\lambda_0)$. Thus, λ_0 is the expansion parameter and it is supposed to be smaller than 1. While the decay parameter γ is defined as $\gamma = \frac{\lambda_0^2}{8\pi m_0}$. Therefore, the value of γ has an allowed region which corresponds $\lambda_0 < 1$.

In our previous work [16], we took $\gamma = 0.1$. This value corresponds to $\lambda_0 \approx 1.58$ and is apparently larger than 1. In such a case, the perturbative solution is no longer consistent with our assumption (i.e., λ_0 is smaller than 1) if we take $\gamma = 0.1$. Let us see what will happen if we take $\gamma = 0.1$ in the numerical calculations.

In Fig. 9, we do the numerical calculations for two cases in which $\gamma = 0.1$ (i.e., equal to $\lambda_0 \approx 1.58$) and $\gamma = 0.000398$ (i.e., equal to $\lambda_0 = 0.1$), with the other parameters $\Omega = 2.3$ and $a = 0.001$ being the same. In the $\gamma = 0.1$ plot, the

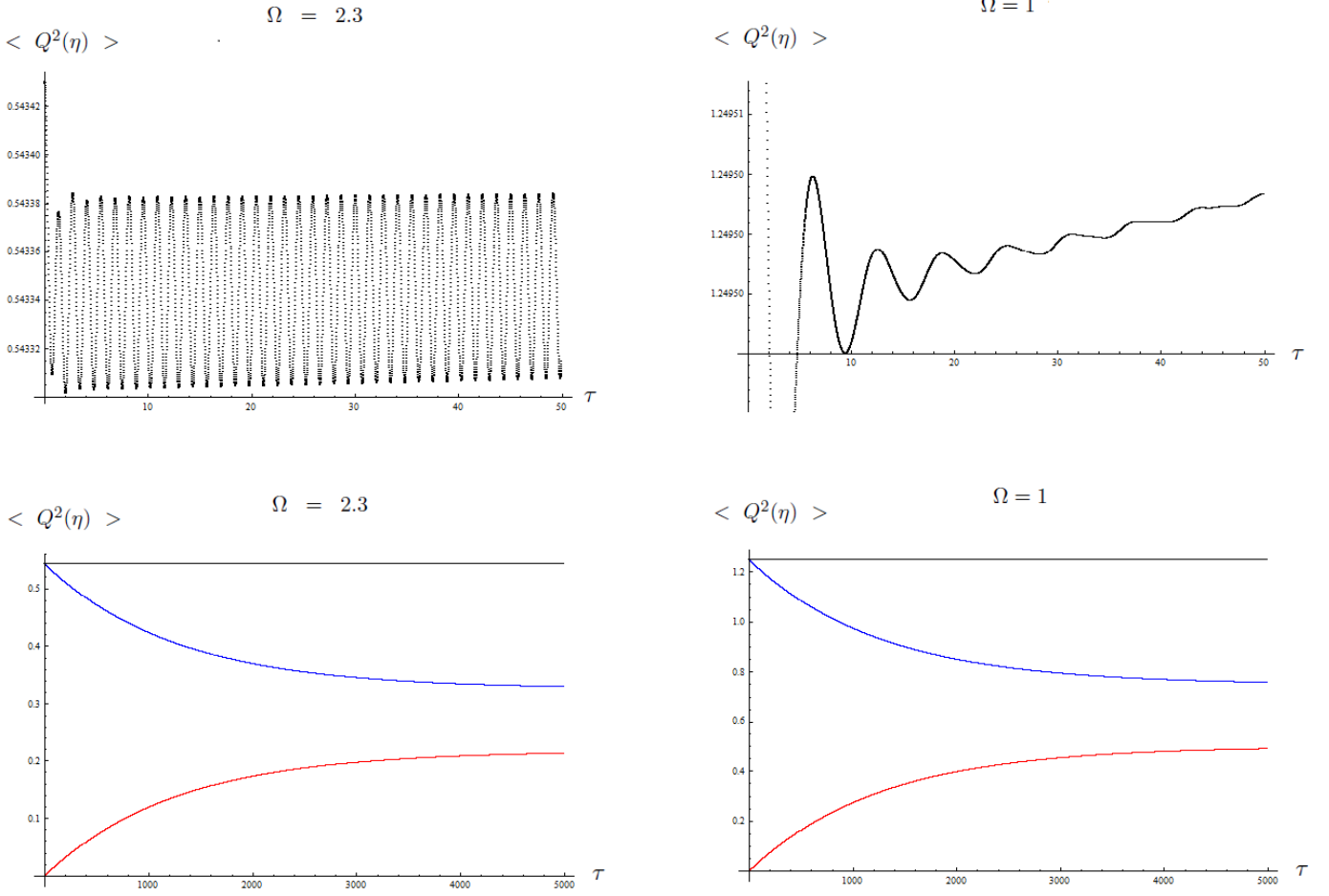


FIG. 5: The frequency Ω . The plot for $\langle Q^2(\eta) \rangle_{v1}$ [red line; Eq. (29) with Λ_0 excluded] and $-\langle Q^2(\eta) \rangle_{v2}$ [blue line; Eq. (30) with $\Lambda_{0,v2}$ excluded], and the sum $\langle Q^2(\eta) \rangle_v$ [black line; which is $\langle Q^2(\eta) \rangle_{v1} - \langle Q^2(\eta) \rangle_{v2}$]. Here $a = 0.001$, $\lambda_0 = 0.1$ ($\gamma = 0.000398$), and $m_0 = \hbar = 1$. Two values of Ω are chosen ($\Omega = 2.3$ and 1.0). The curves arrive at different saturated values for different Ω . The smaller Ω ($\Omega = 1.0$) has a higher saturated value than the bigger Ω ($\Omega = 2.3$) at a later time $\tau = 5000$. When $\tau = 5000$, the final value for $\Omega = 2.3$ is $\langle Q^2(\eta) \rangle_v = 0.543429$, while the final value for $\Omega = 1.0$ is $\langle Q^2(\eta) \rangle_v = 1.24974$. The frequency parameter Ω affects the final saturated value. Also, a bigger Ω has more vibrations in the same τ region and is more active.

missing term $\langle Q^2(\eta) \rangle_{v2}$ (the blue line) becomes unimportant very soon. It drops quickly and then the total effect (the black line) is dominated by the red line $\langle Q^2(\eta) \rangle_{v1}$. The trend of the black line is similar to the red line: both lines are increasing. If we lose the second term $\langle Q^2(\eta) \rangle_{v2}$ in our analytic calculations and then would like to do the numerical integrations at the very beginning as a double check to get a consistent result (meaning the black line and red lines are similar and follow the same trend since the numerical calculation in the beginning does not neglect the missing term and thus will give us the black line), one must set the parameter value at $\gamma = 0.1$ (i.e., $\lambda_0 \approx 1.58$). For $\gamma = 0.1$, the numerical result (black line) will show the same trend as the red line [because the second term $-\langle Q^2(\eta) \rangle_{v2}$ is unimportant for such a γ value]. In short, we must pick a value for γ such that it would make the blue line value small and unimportant. The value $\gamma = 0.1$ fits this goal. And, we would have thought that our analytic results were correct because both analytic and numerical calculations gave us similar curves for the two-point function $\langle Q^2(\eta) \rangle_v$. However, this is just an improper γ value giving us a misleading result. Thus, we must be careful about the allowed and not allowed regions for the parameters in the solutions when we do the numerical calculations as a double check.

Therefore, if one drops the missing term and chooses an allowed γ value, as is shown in Fig. 3 and 4 (i.e., $\gamma = 0.000398$), the trends of the black and the red lines look different—the red line is increasing (with some ripples on it), but the black line looks quite flat. Without noticing the missing term, one may give up this value for γ and go back to the not allowed value of $\gamma = 0.1$ and think that the numerical test is consistent with one's analytic

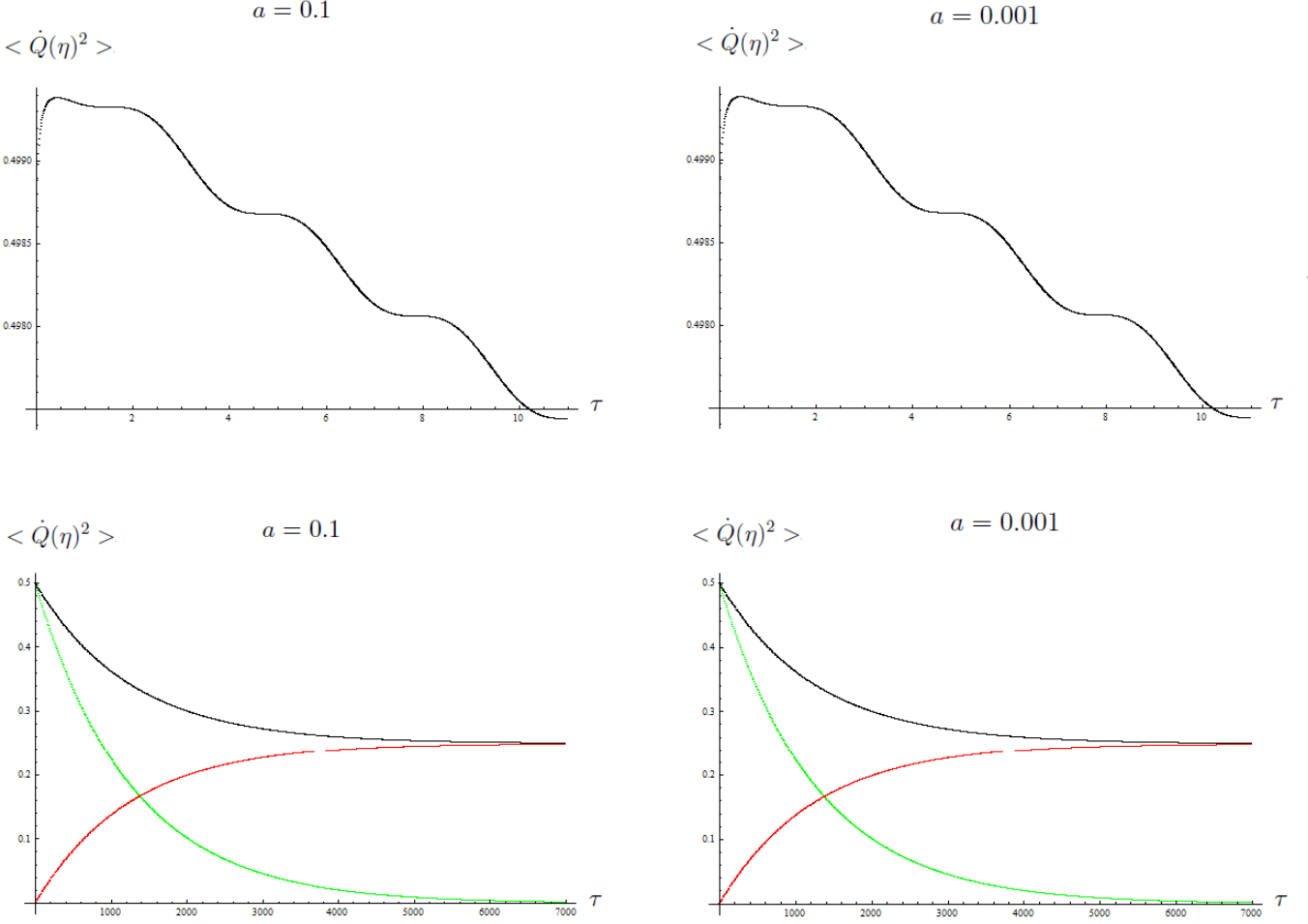


FIG. 6: The proper acceleration a . The plots for $\langle \dot{Q}^2(\eta) \rangle_{v1}$ [red line; Eq. (31) with Λ_1 excluded], $-\langle \dot{Q}^2(\eta) \rangle_{v2}$ [green line; Eq. (32) with $\tilde{\Lambda}_{0,v2}$ excluded], and the sum $\langle \dot{Q}^2(\eta) \rangle_v$ [black line; which is $\langle \dot{Q}^2(\eta) \rangle_{v1} - \langle \dot{Q}^2(\eta) \rangle_{v2}$]. Here $\Omega = 1.0$, $\lambda_0 = 0.1$ (which is $\gamma = 0.000398$), and $m_0 = \hbar = 1$. The green line $-\langle \dot{Q}^2(\eta) \rangle_{v2}$ is larger than $\langle \dot{Q}^2(\eta) \rangle_{v1}$ in the early-time region. The black line oscillates at the beginning and later arrives at the saturated value at around $\tau \approx 6500$. For $\tau = 11$ both the $a = 0.1$ and $a = 0.001$ curves arrive at the same value $\langle \dot{Q}^2(\eta) \rangle_v = 0.497442$. When $\tau = 7000$, the $a = 0.1$ and $a = 0.001$ curves both arrive at the same value $\langle \dot{Q}^2(\eta) \rangle_v = 0.250765$. For $\langle \dot{Q}^2(\eta) \rangle_v$, the difference between the proper accelerations $a = 0.1$ and $a = 0.001$ is not obvious, as shown in the plots. However, the trend of the curve for the two-point function $\langle \dot{Q}^2(\eta) \rangle_v$ is decreasing and differs from the $\langle Q^2(\eta) \rangle_v$ plots.

result (i.e., dropping the missing term). This case may give one's a misleading double check that one's analytic and numerical computations are consistent in terms of the γ value ($\gamma = 0.1$), so one's analytic results are correct. But in fact the contribution of the missing term is suppressed in a not allowed γ region.

In addition, it is important to be careful when choosing a value of a . If we set the light speed $c = 1$, then the proper acceleration a is smaller than 1 (i.e., $a < 1$). In our present numerical calculations, we choose the proper acceleration to be $a = 0.1$ or $a = 0.001$, both of which are smaller than 1. In our previous work, we chose $a = 1$, which is not a good choice if we assume that the light speed $c = 1$. The value $a = 1$ is too large.

Next, we will continue to consider the inertial detector case.

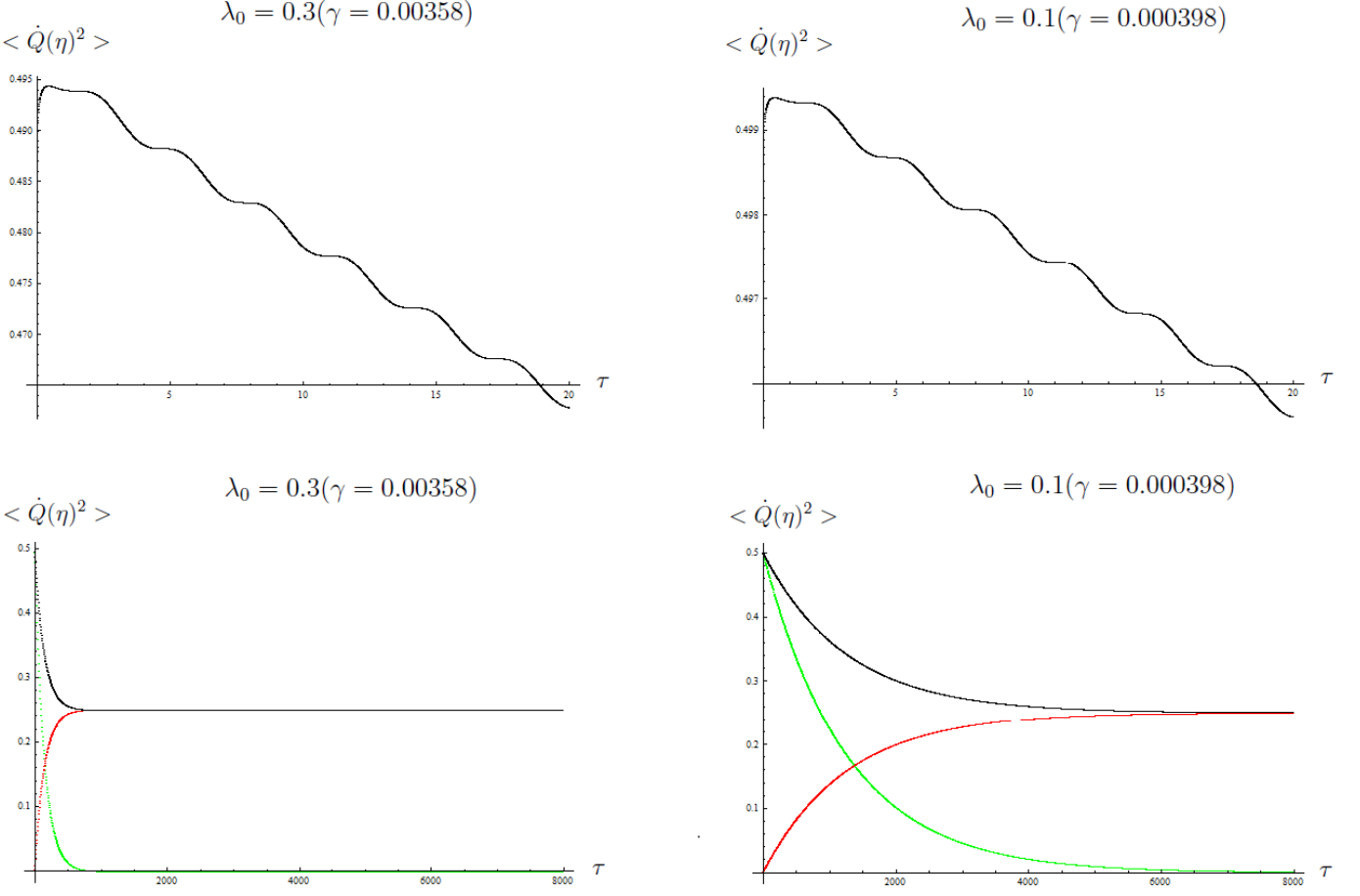


FIG. 7: The decay parameter γ (i.e., the coupling constant λ_0). The plots for $\langle \dot{Q}^2(\eta) \rangle_{v1}$ [red line; Eq. (31) with Λ_1 excluded], $-\langle \dot{Q}^2(\eta) \rangle_{v2}$ [green line; Eq. (32) with $\tilde{\Lambda}_{0,v2}$ excluded], and the sum $\langle \dot{Q}^2(\eta) \rangle_v$ [black line, which is $\langle \dot{Q}^2(\eta) \rangle_{v1} - \langle \dot{Q}^2(\eta) \rangle_{v2}$]. Here $\Omega = 1.0$, $a = 0.1$, and $m_0 = \hbar = 1$. The coupling constants λ_0 differ in these plots. When $\tau = 20$, $\langle \dot{Q}^2(\eta) \rangle_v = 0.4956$ for $\gamma = 0.000398$ and $\langle \dot{Q}^2(\eta) \rangle_v = 0.462788$ for $\gamma = 0.00358$. At a late time when $\tau = 8000$, $\langle \dot{Q}^2(\eta) \rangle_v = 0.250238$ for $\gamma = 0.000398$ and $\langle \dot{Q}^2(\eta) \rangle_v = 0.248185$ for $\gamma = 0.00358$. A larger γ has a higher $\langle \dot{Q}^2(\eta) \rangle_v$ value than a smaller decay parameter γ . The lines oscillate in early-time region and then arrive at a saturated value at a late time. A larger γ decays faster than a smaller γ , and the trend of the $\langle \dot{Q}^2(\eta) \rangle_v$ curve is decreasing except a very short, small rise at the beginning.

C. Trajectory 2 : Inertial detector

We will now calculate the two-point correlation functions $\langle Q^2(\eta) \rangle_v$ and $\langle \dot{Q}^2(\eta) \rangle_v$ for the inertial detector along the trajectory $\tilde{z}_B^\mu = (\gamma\tau, \gamma v\tau + x_a + d, 0, 0)$. This trajectory is for an observer moving at constant velocity and has a finite distance d away from the other static detector. This part differs from that in the previous work that one applies the UAD result and takes the limit $a \rightarrow 0$ to be the result for an inertial detector. In this paper, we have already found that in such a limit $a \rightarrow 0$ the UAD Bob is shifted to very far away and cannot exchange the signal with the inertial detector Alice in a reasonable time interval.

To get the two-point correlation functions for the inertial detector Bob, we simply need to plug the inertial trajectory $\tilde{z}_B^\mu = (\gamma\tau, \gamma v\tau + x_a + d, 0, 0)$ into Eq. (12). Then the difference is that z^0 and \vec{z} in F have changed. As in the derivations of the UAD part, the integral F for this new trajectory \tilde{z}_B^μ is

$$F = \frac{\hbar}{(2\pi)^3} \int_0^{2\pi} d\phi \int_{-1}^1 d(\cos\theta) \int_0^\infty \frac{\omega^2 d\omega}{2\omega} \int_{-\infty}^\infty \frac{dt}{2\pi} \int_{-\infty}^\infty \frac{dt'}{2\pi} e^{i\kappa t - i\kappa' t' - i\omega(z^0(t) - z^0(t')) + i\omega \cos\theta |\vec{z} - \vec{z}'|}$$

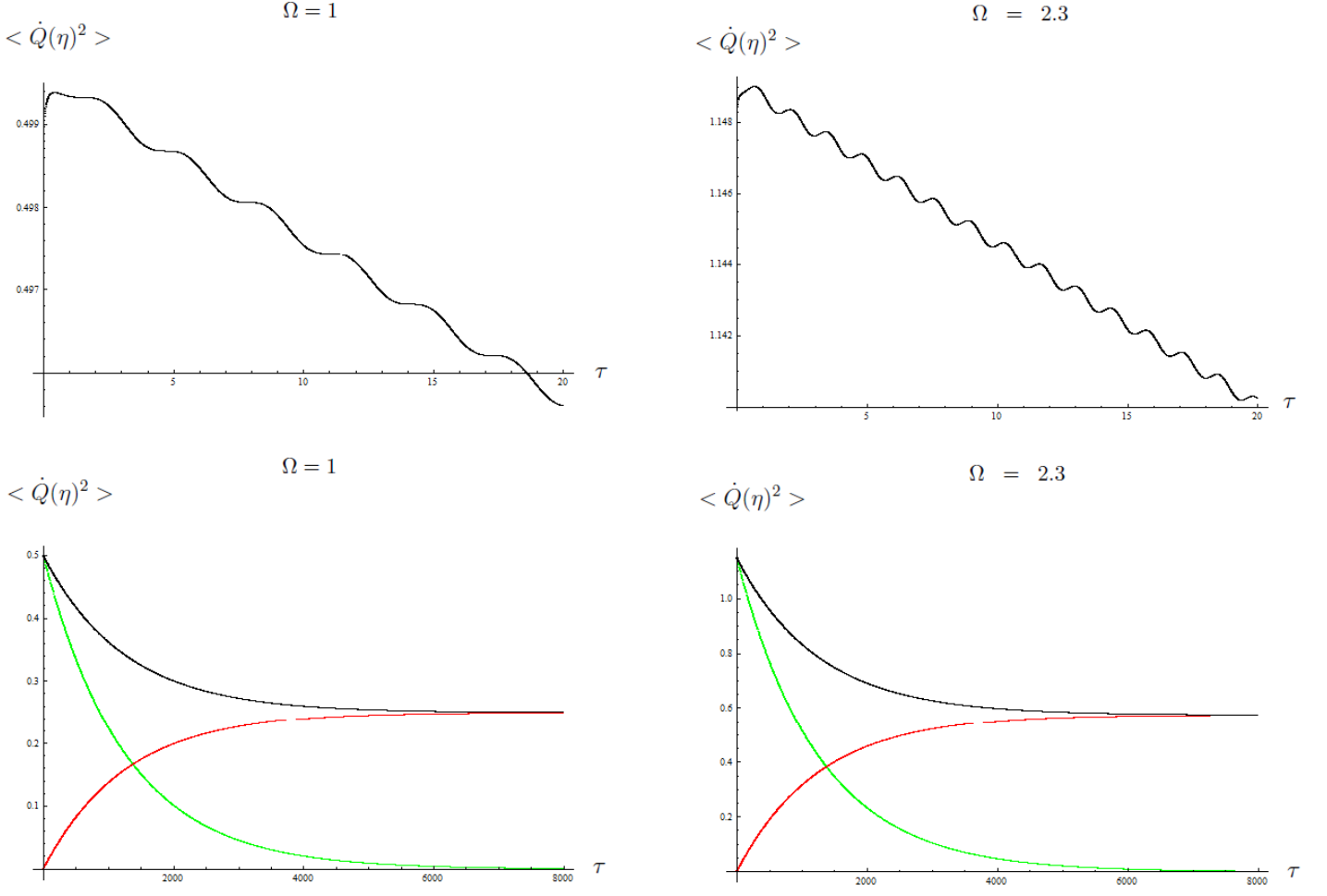


FIG. 8: The frequency parameter Ω . The plots for $\langle Q^2(\eta) \rangle_{v1}$ [red line; Eq. (31) with Λ_1 excluded], and $-\langle Q^2(\eta) \rangle_{v2}$ [green line, Eq.(32) with Λ_{0v2} excluded], and the sum $\langle Q^2(\eta) \rangle_v$ [black line, which is $\langle Q^2(\eta) \rangle_{v1} - \langle Q^2(\eta) \rangle_{v2}$]. Here $a = 0.1$, $\gamma = 0.000398$ ($\lambda_0 = 0.1$) and $m_0 = \hbar = 1$. A larger Ω has a higher value for the two-point function $\langle Q^2(\eta) \rangle_v$. The black line has a small rise in the beginning and then decreases to a saturated value. A larger Ω has more oscillations in the same time interval as a smaller Ω . The magnitude of Ω alters the intensity of the two-point function $\langle Q^2(\eta) \rangle_v$.

$$\begin{aligned}
&= \frac{\hbar}{2\pi} \int_0^\infty d\omega \int_{-\infty}^\infty \frac{dt}{2\pi} \int_{-\infty}^\infty \frac{dt'}{2\pi} e^{i\kappa t - i\kappa' t' - i\omega[z^0(t) - z^0(t')]} \frac{\sin(\omega|\vec{z}(t) - \vec{z}(t')|)}{|\vec{z}(t) - \vec{z}(t')|} \\
&= \frac{\hbar}{(2\pi)^4} \int_{-\infty}^\infty dt \int_{-\infty}^\infty dt' \frac{e^{i\kappa(t - \frac{i\epsilon}{2}) - i\kappa'(t' + \frac{i\epsilon}{2})}}{|\vec{z}(t - \frac{i\epsilon}{2}) - \vec{z}(t' + \frac{i\epsilon}{2})|^2 - [z^0(t - \frac{i\epsilon}{2}) - z^0(t' + \frac{i\epsilon}{2})]^2} \\
&= \frac{\hbar}{(2\pi)^4} \int_{-\infty}^\infty dt \int_{-\infty}^\infty dt' \frac{e^{\frac{\epsilon}{2}(\kappa + \kappa') + i\kappa t - i\kappa' t'}}{\gamma^2(\tau - \tau' - i\epsilon)^2(v^2 - 1)} \\
&= \frac{\hbar}{(2\pi)^4} \int_{-\infty}^\infty dT \int_{-\infty}^\infty d\Delta \frac{e^{\frac{\epsilon}{2}(\kappa + \kappa') + i(\kappa - \kappa')T + \frac{i\Delta}{2}(\kappa + \kappa')}}{-(\Delta - i\epsilon)^2} \\
&= \frac{\hbar}{(2\pi)^3} \delta(\kappa - \kappa') \int_{-\infty}^\infty d\Delta \frac{e^{\kappa\epsilon} e^{i\kappa\Delta}}{-(\Delta - i\epsilon)^2} \\
&= \frac{\hbar}{(2\pi)^2} \delta(\kappa - \kappa') \kappa, \quad \kappa \geq 0.
\end{aligned} \tag{33}$$

Note that $F = 0$ when $\kappa < 0$. The velocity v is canceled out in the denominator and does not appear in the integration term F , which implies that, no matter how fast or slow the velocity is, the result for F is the same.

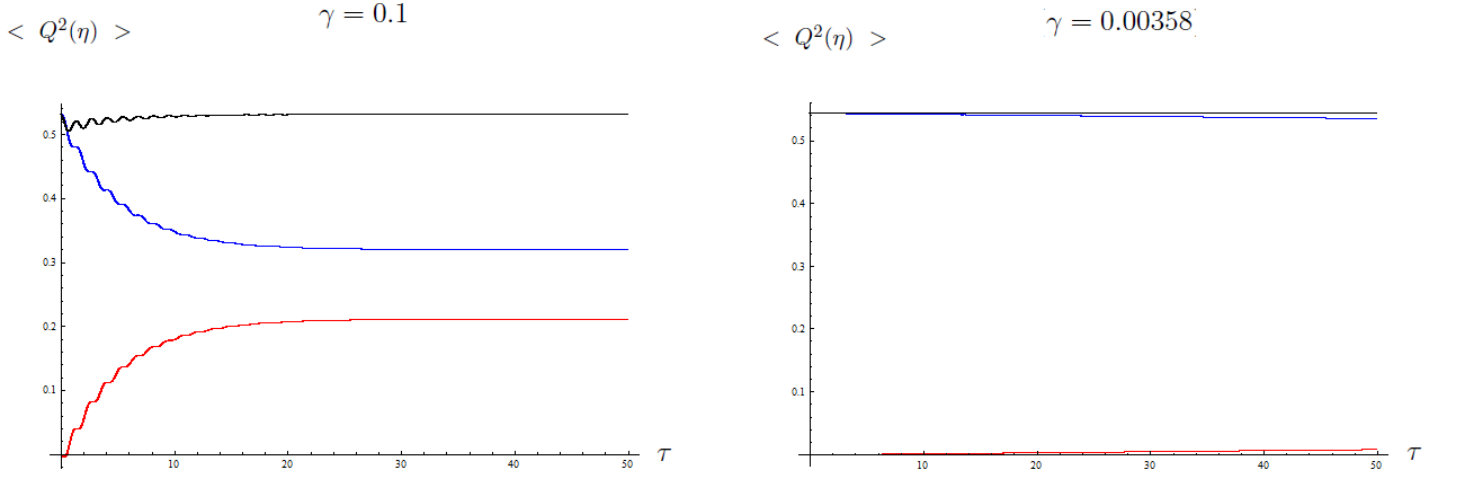


FIG. 9: The plots for the proper and improper γ values. The plots for $\langle Q^2(\eta) \rangle_{v1}$ [red line, Eq. (31) with Λ_1 excluded], $-\langle Q^2(\eta) \rangle_{v2}$ [green line, Eq. (32) with $\tilde{\Lambda}_{0v2}$ excluded], and the sum $\langle Q^2(\eta) \rangle_v$ [black line, which is $\langle Q^2(\eta) \rangle_{v1} - \langle Q^2(\eta) \rangle_{v2}$]. Here $a = 0.001$, $\Omega = 2.3$ and $m_0 = \hbar = 1$. $\gamma = 0.1$ is the improper γ value, while $\gamma = 0.000398$ is the proper value.

As in Eq. (16), plugging F back into the two-point function $\langle Q(\tau - \tau_0)Q(\tau'' - \tau_0'') \rangle_v$ and performing the integration of τ , we have the two-point function for the inertial detector

$$\begin{aligned} & \langle Q(\tau - \tau_0)Q(\tau'' - \tau_0'') \rangle_v \\ &= \frac{\lambda_0^2 \hbar}{(2\pi)^2 m_0^2} \sum_{j,j'} \int_0^\infty \kappa d\kappa \frac{c_j c_{j'}^* e^{-i\kappa(\tau_0 - \tau_0'')}}{(w_j + i\kappa)(w_{j'}^* - i\kappa)} (e^{w_j(\tau - \tau_0)} - e^{-i\kappa(\tau - \tau_0)}) \cdot (e^{w_{j'}^*(\tau'' - \tau_0'')} - e^{-i\kappa(\tau'' - \tau_0'')}). \end{aligned} \quad (34)$$

Performing the κ integration and then using the same calculation steps for the uniformly accelerated detector that we used previously in the paper, we obtain the following result for the two-point correlation function of the internal degrees of freedom Q for the inertial detector Bob

$$\begin{aligned} & \langle Q(\eta)^2 \rangle_v \equiv \lim_{\eta'' \rightarrow \eta} \frac{1}{2} \langle \{Q(\eta), Q(\eta'')\} \rangle_v \\ &= \frac{2\hbar\gamma}{\pi m_0} \theta(\eta) \text{Re} \left\{ \tilde{\Lambda}_0 + \frac{e^{-2\gamma(\tau - \tau_0)}}{8\Omega^2} \left[\left(1 - \frac{i\Omega}{\gamma} - e^{2i\Omega(\tau - \tau_0)} \right) (i\pi - 2 \log(\gamma - i\Omega) + \Gamma(0, (-\gamma + i\Omega)(\tau - \tau_0))) \right. \right. \\ & \quad \left. \left. + \left(1 + \frac{i\Omega}{\gamma} - e^{-2i\Omega(\tau - \tau_0)} \right) (-3i\pi - 2 \log(\gamma + i\Omega) + \Gamma(0, -(\gamma + i\Omega)(\tau - \tau_0))) \right] + \frac{i}{8\Omega\gamma} \right. \\ & \quad \left. \cdot [-2i\pi + 2 \log(\gamma - i\Omega) - 2 \log(\gamma + i\Omega) - \Gamma(0, (\gamma - i\Omega)(\tau - \tau_0)) + \Gamma(0, (\gamma + i\Omega)(\tau - \tau_0))] \right\}, \end{aligned} \quad (35)$$

where $\tilde{\Lambda}_0$ contains divergent parts [i.e., $\Gamma(0, 0)$ and $\log(0)$] as $\tau'' \rightarrow \tau$ and $\tau_0'' \rightarrow \tau_0$ and are absorbed into the renormalized constant or coefficient in the experiment.

Similarly, the result of $\langle \dot{Q}(\eta)^2 \rangle_v$ as

$$\begin{aligned} & \langle \dot{Q}(\eta)^2 \rangle_v \equiv \lim_{\eta'' \rightarrow \eta} \frac{1}{2} \langle \{\dot{Q}(\eta), \dot{Q}(\eta'')\} \rangle_v \\ &= \frac{2\hbar\gamma}{\pi m_0} \theta(\eta) \text{Re} \left\{ \tilde{\Lambda}_{0v} + \frac{e^{-2\gamma(\tau - \tau_0)}}{8\Omega^2} \left[\left(\frac{(\gamma - i\Omega)(\gamma^2 + \Omega^2)}{\gamma} - (\gamma - i\Omega)^2 e^{2i\Omega(\tau - \tau_0)} \right) (-i\pi - 2 \log(\gamma - i\Omega)) \right. \right. \\ & \quad \left. \left. + \left(\frac{(\gamma + i\Omega)(\gamma^2 + \Omega^2)}{\gamma} - (\gamma + i\Omega)^2 e^{-2i\Omega(\tau - \tau_0)} \right) (-i3\pi - 2 \log(\gamma + i\Omega)) \right] \right. \\ & \quad \left. + \frac{e^{(-\gamma + i\Omega)(\tau - \tau_0)}}{8\Omega^2} \left[\gamma - i\Omega - \frac{(\gamma - i\Omega)^2}{\gamma} \right] \left[\frac{2}{\tau - \tau_0} - 2(\gamma - i\Omega) e^{(\gamma - i\Omega)(\tau - \tau_0)} \Gamma(0, (\gamma - i\Omega)(\tau - \tau_0)) \right] \right\} \end{aligned}$$

$$\begin{aligned}
& + \frac{e^{(-\gamma-i\Omega)(\tau-\tau_0)}}{8\Omega^2} \left[\gamma + i\Omega - \frac{(\gamma + i\Omega)^2}{\gamma} \right] \left[\frac{2}{\tau - \tau_0} - 2(\gamma + i\Omega)e^{(\gamma+i\Omega)(\tau-\tau_0)}\Gamma(0, (\gamma + i\Omega)(\tau - \tau_0)) \right] \\
& + \frac{e^{-\gamma(\tau-\tau_0)}}{8\Omega^2} \left[(-2i \sin(\Omega(\tau - \tau_0)) + \frac{i\Omega}{\gamma}e^{i\Omega(\tau - \tau_0)}) \left[\frac{2(\gamma + i\Omega)}{\tau - \tau_0} - 2(\gamma + i\Omega)^2e^{-(\gamma+i\Omega)(\tau-\tau_0)}(i\pi \right. \right. \\
& \left. \left. - \Gamma(0, -(\gamma + i\Omega)(\tau - \tau_0))) \right] + (2i \sin(\Omega(\tau - \tau_0)) - \frac{i\Omega}{\gamma}e^{-i\Omega(\tau - \tau_0)}) \left[\frac{2(\gamma - i\Omega)}{\tau - \tau_0} \right. \right. \\
& \left. \left. + 2(\gamma - i\Omega)^2e^{-(\gamma-i\Omega)(\tau-\tau_0)} \cdot (i\pi + \Gamma(0, -(\gamma - i\Omega)(\tau - \tau_0))) \right] \right] + \frac{i}{8\Omega\gamma} \cdot \\
& \left[-(\gamma - i\Omega)^2(2 \log(\gamma - i\Omega) - i\pi) + (\gamma + i\Omega)^2(2 \log(\gamma + i\Omega) + i\pi) \right], \tag{36}
\end{aligned}$$

where $\tilde{\Lambda}_{0v}$ contains divergent parts[i.e., $\Gamma(0, 0)$ and $\log(0)$] as $\tau'' \rightarrow \tau$ and $\tau_0'' \rightarrow \tau_0$ that are absorbed into the renormalized constant or coefficient in the experiment.

Note that the condition $\kappa \geq 0$ is very important. If one does not notice that $\kappa \geq 0$ and takes the integration region of κ from $-\infty$ to ∞ in Eq. (34)[i.e., $\int_{-\infty}^{+\infty} \kappa d\kappa f(\kappa)$], one will have $\langle Q(\eta)^2 \rangle_v = 0$ in Eq. (35) for the inertial detector. This implies that the variance from the background quantum field is zero, which is highly unlikely because a quantum field always contributes a nonzero variance. Actually, this strange result is the motivation for our rechecking the two-point function $\langle Q(\eta)^2 \rangle_v$ for the UAD and inertial detectors. An interesting point is that Eq. (34) can be reshaped in the form of Eq. (28)[i.e., $\int_0^{+\infty} \kappa d\kappa f(\kappa) = \int_{-\infty}^{+\infty} \kappa d\kappa f(\kappa) - \int_{-\infty}^0 \kappa d\kappa f(\kappa)$]; thus, the two-point function $\langle Q(\eta)^2 \rangle_v$ is now nonzero, and the variance for the inertial detector is nonzero if we insist on taking the integration region of κ as $\int_{-\infty}^{+\infty} \kappa d\kappa f(\kappa)$ (i.e., this integration region is what we applied in the previous calculations). Therefore we think that the second term $\langle Q(\eta)^2 \rangle_{v2}$ is the missing term and is important when we talk about the variance from the background quantum field for the inertial detector. The missing term also changes the trend for the two-point function $\langle \dot{Q}(\eta)^2 \rangle_v$ curve in the UAD case, as shown previously. Later, we will plot the curves of the two-point functions $\langle Q(\eta)^2 \rangle_v$ and $\langle \dot{Q}(\eta)^2 \rangle_v$ for the inertial detector.

The numerical plots for $\langle Q(\eta)^2 \rangle_v$ and $\langle \dot{Q}(\eta)^2 \rangle_v$ are shown in Fig. 10 and 11. The values for the two-point functions $\langle Q(\eta)^2 \rangle_v$ and $\langle \dot{Q}(\eta)^2 \rangle_v$ follow the same trend. The value first increase slowly with ripples on the curve, and then reach a saturated value. This differs from the UAD case; for example, in Fig. 3, the amplitude of the ripples gradually becomes small. For the UAD case, the early amplitude is larger than the later amplitudes. Note that the value for the two-point correlation functions of UAD changes only slightly relative to the inertial detector. The curve for UAD is quite flat. The magnitude of $\langle Q(\eta)^2 \rangle_v$ for the inertial detector has an obvious change from the beginning to the end. Besides, the ripples on the inertial detector curve of the two-point function $\langle Q(\eta)^2 \rangle_v$ has the same oscillating amplitude on the ripples until it reaches the saturated value. The effect of acceleration is clear in the early-time region if we compare the UAD detector curve to the inertial detector curve.

Fig. 11 shows $\langle \dot{Q}(\eta)^2 \rangle$ for an inertial detector. When we compare it to the Fig. 6 [i.e., $\langle \dot{Q}(\eta)^2 \rangle$ for UAD], the curve for UAD decreases to a saturated value, which differs from the inertial case. This feature can be seen with the term $\langle Q(\eta)^2 \rangle$; for example, in Fig. 3 the amplitude of the oscillations gradually become small, which implies that the changes of $\langle \dot{Q}(\eta)^2 \rangle$ also become small as τ increases. A clear feature of a UAD is that its magnitude of $\langle \dot{Q}(\eta)^2 \rangle$ decreases in the early-time region.

In Figs. 3- 11 we can see that the difference between the inertial detector and the UAD is clear in the plots for the two-point correlation functions $\langle Q(\eta)^2 \rangle$ and $\langle \dot{Q}(\eta)^2 \rangle$. For the two-point function $\langle Q(\eta)^2 \rangle$ of the UAD, the curve has larger oscillations at first and then experiences smaller oscillations, and the magnitude does not change much from beginning to the end. On the contrary, the amplitude of the oscillations of the two-point function $\langle Q(\eta)^2 \rangle$ for the inertial detector does not shrink in the beginning, and the magnitude increases from the beginning until it reaches the saturated region. For the two-point function $\langle \dot{Q}(\eta)^2 \rangle$, the difference between the UAD and the inertial detector is more obvious that the curve for $\langle \dot{Q}(\eta)^2 \rangle$ of the UAD decreases to a saturated value, while the curve for the inertial detector increases. The effect of proper acceleration is evident in the two-point correlation functions $\langle Q(\eta)^2 \rangle$ and $\langle \dot{Q}(\eta)^2 \rangle$. We think that the difference is from the Unruh effect in that the uniformly accelerated detector would experience a thermal bath at temperature $T_U = \hbar a / (2\pi c k_B)$, where a is the proper acceleration. This thermal bath changes the two-point correlation functions.

IV. SUMMARY

In this paper, we investigate the two moving detectors Alice and Bob in a quantum field. In this system, Alice is static while Bob either accelerates uniformly or moves at a constant velocity. We apply two different types of

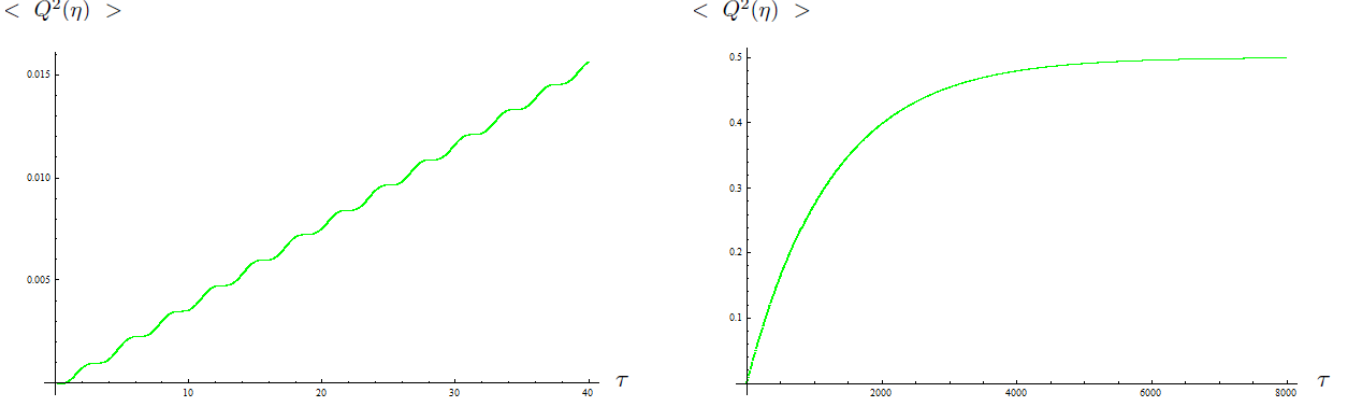


FIG. 10: The two-point correlation function $\langle Q(\eta)^2 \rangle_v$ for an inertial detector. Here $a = 0.001$, $\gamma = 0.000398(\lambda_0 = 0.1)$, $m_0 = \hbar = 1$, and $\Omega = 1$. Two different timescales are shown. The value increases slowly in the beginning with ripples on the curve, then reaches a saturated value later.

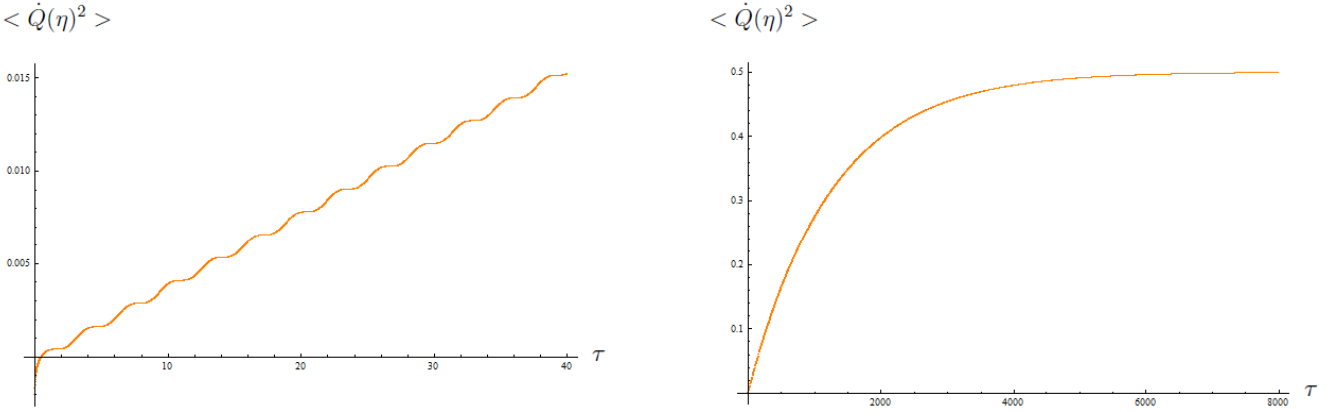


FIG. 11: The two-point correlation function $\langle \dot{Q}(\eta)^2 \rangle$ for an inertial detector. Here $a = 0.001$, $\gamma = 0.000398(\lambda_0 = 0.1)$, $m_0 = \hbar = 1$, and $\Omega = 1$. These plots are similar to those for the $\langle Q(\eta)^2 \rangle$ case. Two different timescales are shown. The value of the two-point function increases slowly in the beginning with ripples on the curve, and then reaches a saturated value later.

trajectories for such a setup and calculate the solutions for the internal degrees of freedom Q for the moving detector Bob under the influence of the background quantum field. In this work, we find the following points:

(1) The inertial worldline that we need for two moving detectors to exchange the signals within a reasonable finite time interval cannot be replaced by the UAD trajectory in Rindler space $z_B^\mu = (a^{-1} \sinh a\tau, a^{-1} \cosh a\tau, 0, 0)$ by setting the proper acceleration $a = 0$. When the proper acceleration in the Rindler space goes to zero, the UAD worldline is shifted to very far away such that Alice and Bob no longer exchange signals within a reasonable time interval. Therefore, we need to apply a true trajectory $\tilde{z}_B^\mu = (\gamma\tau, \gamma v\tau + x_a + d, 0, 0)$ for a detector moving at constant velocity. By using the trajectory \tilde{z}_B^μ , Bob is separated from Alice at the distance "d" in the beginning so that they can exchange the signal in a finite time interval. We can apply this trajectory to compute the two-point functions $\langle Q(\eta)^2 \rangle$ and $\langle \dot{Q}(\eta)^2 \rangle$ for the inertial detector, then compare the two-point correlation functions $\langle Q(\eta)^2 \rangle$ and $\langle \dot{Q}(\eta)^2 \rangle$ for the UAD and inertial detector.

(2) We find that a term was missing from both two-point correlation functions $\langle Q(\eta)^2 \rangle_v$ and $\langle \dot{Q}(\eta)^2 \rangle_v$ in the previous calculations. Without this term, the variance from the background quantum field part of the inertial detector is "0" [i.e., $\langle Q(\eta)^2 \rangle_v = 0$], which is highly unlikely. However, if the missing term is included, the variance from the background quantum field for the inertial detector is nonzero, which is what we expect when a moving detector

interacts with a quantum field. The missing term also changes the behavior of the two-point correlation functions $\langle Q(\eta)^2 \rangle_v$ and $\langle \dot{Q}(\eta)^2 \rangle_v$ for UAD; this point was not noticed previously.

(3) The values of the parameters in this model are in an allowed region. We apply the perturbation method to obtain the solutions for Q ; therefore, the parameters in this model should obey the basic assumption for perturbations that the next leading order must be smaller than the leading order. In the previous work, we did not notice this and took the decay parameter γ to be $\gamma = 0.1$, which means that the expansion parameter λ_0 is larger than 1 (when $\gamma = 0.1$, the coupling constant $\lambda_0 \simeq 1.58$). This value of γ is inconsistent with the basic assumption of the perturbation and will give us an artefact. And this will lead to misleading results pertaining to the effects of proper acceleration.

(4) Including the above considerations, the UAD and inertial detector result in different behaviors in $\langle Q(\eta)^2 \rangle_v$ and $\langle \dot{Q}(\eta)^2 \rangle_v$. In the early-time region the two-point function $\langle Q(\eta)^2 \rangle_v$ for UAD has a quite flat curve, while the inertial detector has an increasing curve. The amplitude of those oscillations on the ripples of the UAD curve gradually shrinks, while the amplitude of the oscillations on the ripples of the inertial detector does not change. For the two-point function $\langle \dot{Q}(\eta)^2 \rangle_v$, the difference is more clear than it is for $\langle Q(\eta)^2 \rangle_v$. The curve for $\langle \dot{Q}(\eta)^2 \rangle_v$ of the UAD is high at first and then decreases until it reaches the saturated value. However, the curve of $\langle \dot{Q}(\eta)^2 \rangle_v$ for the inertial detector increases until it reaches the saturated value. This part is quite different from the previous result. We think that this implies that the proper acceleration a has some effect on the vacuum state of Q and thus affects the vacuum fluctuations of the UAD (the Unruh effect).

The foundations of the calculations were built by Lin and Hu [16], who used the quantum field theory method and then applied it to the two moving detectors system by Lin *et al.* [17]. These are not easy calculations. Here, based on their work, we redo the calculations and modify them. Since the calculation is tricky, we write the detailed calculations here for those who are interested.

In the future, we would like to apply these results to the quantum teleportation issue, for example, the two moving detector system in which Alice and Bob have relativistic motion with each other. We would like to see whether the Unruh effect may play a role in the quantum teleportation process for two relatively moving detectors.

V. ACKNOWLEDGEMENT

We would like to thank Dr. Shih-Yuin Lin, Dr. Chung-Hsien Chou, Dr. Jen-Tsung Hsiang and Dr. Ron-Chou Hsieh for helpful discussions, and Professor Bei-Lok Hu and Professor Kin-Wang Ng for the encouragement and help. Special thanks are given to Dr. Shih-Yuin Lin for providing some detailed notes about the calculations of the two-point functions. This work is supported in part by the Ministry of Science and Technology, Taiwan under Grants No. MOST 106-2811-M-108-006 and No. MOST 109-2112-M-001-003.

APPENDIX A: QUANTIZATION

We quantize the field Φ and the harmonic oscillators Q_A, Q_B in the Heisenberg picture. The conjugate momentum $(P(\tau), \Pi(x))$ of these canonical coordinate and momentum $(Q(\tau), \Phi(x))$ are

$$P_d(\tau) = \frac{\delta S}{\delta \dot{Q}_d(\tau)} = \dot{Q}_d(\tau), \quad d = A, B, \quad (37)$$

$$\Pi(\tau) = \frac{\delta S}{\delta \partial_t \Phi(x)} = \partial_t \Phi(x). \quad (38)$$

The equal time commutation relations of these dynamical variables are

$$[\hat{Q}_d(\tau), \hat{P}_d(\tau)] = i\hbar, \quad d = A, B; \quad (39)$$

$$[\hat{\Phi}(t, \mathbf{x}), \hat{\Pi}(t, \mathbf{x}')] = i\hbar \delta^3(\mathbf{x} - \mathbf{x}'). \quad (40)$$

According to the Heisenberg equations of motion, one can write the equation of motions for \hat{Q} and $\hat{\Phi}$ as

$$\partial_\tau^2 \hat{Q}_d(\tau) + \Omega_0^2 \hat{Q}_d(\tau) = \lambda_0 \hat{\Phi}_d(\tau, \mathbf{z}(\tau)), \quad d = A, B, \quad (41)$$

$$(\partial_t^2 - \nabla^2) \hat{\Phi}_d(x) = \lambda_0 \int_0^\infty d\tau \hat{Q}_d(\tau) \delta^4(x - z(\tau)). \quad (42)$$

The operators $\hat{Q}_d(\tau_d)$ and $\hat{\Phi}_d(x_d)$ are expanded by the mode functions and the creation(annihilation) operators as

$$\hat{Q}_i(\tau_i) = \sqrt{\frac{\hbar}{2\Omega_r}} \sum_j \left[q_i^{(j)}(\tau_i) \hat{a}_j + q_i^{(j)*}(\tau_i) \hat{a}_j^\dagger \right] + \int \frac{d^3 k}{(2\pi)^3} \sqrt{\frac{\hbar}{2\omega}} \left[q_i^{(+)}(\tau_i, \mathbf{k}) \hat{v}_{\mathbf{k}} + q_i^{(-)}(\tau_i, \mathbf{k}) \hat{v}_{\mathbf{k}}^\dagger \right], \quad (43)$$

$$\hat{\Phi}(x) = \sqrt{\frac{\hbar}{2\Omega_r}} \sum_j \left[f^{(j)}(x) \hat{a}_j + f^{(j)*}(x) \hat{a}_j^\dagger \right] + \int \frac{d^3 k}{(2\pi)^3} \sqrt{\frac{\hbar}{2\omega}} \left[f^{(+)}(x, \mathbf{k}) \hat{v}_{\mathbf{k}} + f^{(-)}(x, \mathbf{k}) \hat{v}_{\mathbf{k}}^\dagger \right], \quad (44)$$

where $i, j = A, B$, $\tau_A = t$, $\tau_B = \tau$, $q_i^{(j)}$, $q_i^{(\pm)}$, $f^{(j)}$, and $f^{(\pm)}$ are the c -number mode functions. The conjugate momenta are $\hat{P}_A(t) = \partial_t \hat{Q}_A(t)$, $\hat{P}_B(\tau) = \partial_\tau \hat{Q}_B(\tau)$, and $\hat{\Pi}(x) = \partial_t \hat{\Phi}(x)$. The equations of motion for the mode functions are as follows:

$$(\partial_{\tau_i}^2 + \Omega_0^2) q_i^{(j)}(\tau_i) = \lambda_0 f^{(j)}(z_i^\mu(\tau_i)), \quad (45)$$

$$(\partial_t^2 - \nabla^2) f^{(j)}(x) = \lambda_0 \left[\int_0^\infty dt q_A^{(j)} \delta^4(x - z_A(t)) + \int_0^\infty d\tau q_B^{(j)} \delta^4(x - z_B(\tau)) \right], \quad (46)$$

$$(\partial_{\tau_i}^2 + \Omega_0^2) q_i^{(+)}(\tau_i, \mathbf{k}) = \lambda_0 f^{(+)}(z_i^\mu(\tau_i), \mathbf{k}), \quad (47)$$

$$(\partial_t^2 - \nabla^2) f^{(+)}(x, \mathbf{k}) = \lambda_0 \left[\int_0^\infty dt q_A^{(+)}(t, \mathbf{k}) \delta^4(x - z_A(t)) + \int_0^\infty d\tau q_B^{(+)}(\tau, \mathbf{k}) \delta^4(x - z_B(\tau)) \right]. \quad (48)$$

APPENDIX B: THE EQUATIONS OF MOTION, MODE FUNCTIONS AND STATES

The equations of motion of one moving detector for the Lagrangian in Eq. (8) are as follows:

$$\partial_\tau^2 \hat{Q}(\tau) + \Omega_0^2 \hat{Q}(\tau) = \lambda_0 \hat{\Phi}(\tau, \mathbf{z}(\tau)), \quad (49)$$

$$(\partial_t^2 - \nabla^2) \hat{\Phi}(x) = \lambda_0 \int_0^\infty d\tau \hat{Q}(\tau) \delta^4(x - z(\tau)). \quad (50)$$

We assume that the system is prepared before $\tau = 0$ and that the coupling is turned on at $\tau = 0$ when we allow all the dynamical variables to begin to interact and evolve under the influence of one another. The time evolution of $\hat{\Phi}(x)$ is a linear transformation in the phase space spanned by the orthonormal basis $(\hat{\Phi}(\mathbf{x}), \hat{\Pi}(\mathbf{x}), \hat{Q}, \hat{P})$, and $\hat{\Phi}(x)$ can be expressed in the form

$$\hat{\Phi}(t, \mathbf{x}) = \int d^3 x' \left[f^\Phi(t, \mathbf{x}, \mathbf{x}') \hat{\Phi}(0, \mathbf{x}') + f^\Pi(t, \mathbf{x}, \mathbf{x}') \hat{\Pi}(0, \mathbf{x}') \right] + f^Q(x) \hat{Q}(0) + f^P(x) \hat{P}(0). \quad (51)$$

Here $f^\Phi(x, \mathbf{x}')$, $f^\Pi(x, \mathbf{x}')$, $f^Q(x)$ and $f^P(x)$ are c -number functions. Similarly, the operator $\hat{Q}(\tau)$ can be expressed as follows:

$$\hat{Q}(\tau) = \int d^3 x' \left[q^\Phi(\tau, \mathbf{x}') \hat{\Phi}(0, \mathbf{x}') + q^\Pi(\tau, \mathbf{x}') \hat{\Pi}(0, \mathbf{x}') \right] + q^Q(\tau) \hat{Q}(0) + q^P(\tau) \hat{P}(0), \quad (52)$$

with c -number functions $q^Q(\tau)$, $q^P(\tau)$, $q^\Phi(\tau, \mathbf{x}')$ and $q^\Pi(\tau, \mathbf{x}')$.

For the case in which initial operators are the free field operators, namely, $\hat{\Phi}(0, \mathbf{x}) = \hat{\Phi}_0(\mathbf{x})$, $\hat{\Pi}(0, \mathbf{x}) = \hat{\Pi}_0(\mathbf{x})$, $\hat{Q}(0) = \hat{Q}_0$ and $\hat{P}(0) = \hat{P}_0$, one can go further by introducing the following complex operators $\hat{v}_{\mathbf{k}}$ and \hat{a} :

$$\hat{\Phi}_0(\mathbf{x}) = \int \frac{d^3 k}{(2\pi)^3} \sqrt{\frac{\hbar}{2\omega}} \left[e^{i\mathbf{k}\cdot\mathbf{x}} \hat{v}_{\mathbf{k}} + e^{-i\mathbf{k}\cdot\mathbf{x}} \hat{v}_{\mathbf{k}}^\dagger \right], \quad (53)$$

$$\hat{\Pi}_0(\mathbf{x}) = \int \frac{d^3 k}{(2\pi)^3} \sqrt{\frac{\hbar}{2\omega}} (-i\omega) \left[e^{i\mathbf{k}\cdot\mathbf{x}} \hat{v}_{\mathbf{k}} - e^{-i\mathbf{k}\cdot\mathbf{x}} \hat{v}_{\mathbf{k}}^\dagger \right] \quad (54)$$

with $\omega \equiv |\mathbf{k}|$, and

$$\hat{Q}_0 = \sqrt{\frac{\hbar}{2\Omega_r m_0}}(\hat{a} + \hat{a}^\dagger), \quad \hat{P}_0 = -i\sqrt{\frac{\hbar\Omega_r m_0}{2}}(\hat{a} - \hat{a}^\dagger). \quad (55)$$

Note that, instead of Ω_0 , we use the renormalized natural frequency Ω_r [to be defined in Eq. (89)] in the definition of \hat{a} . Then the commutation relations (39) and (40) give

$$[\hat{a}, \hat{a}^\dagger] = 1, \quad [\hat{v}_{\mathbf{k}}, \hat{v}_{\mathbf{k}'}^\dagger] = (2\pi)^3 \delta^3(\mathbf{k} - \mathbf{k}'), \quad (56)$$

and the expressions (51) and (52) can be rewritten as

$$\hat{\Phi}(t, \mathbf{x}) = \hat{\Phi}_v(x) + \hat{\Phi}_a(x), \quad (57)$$

$$\hat{Q}(\tau) = \hat{Q}_v(\tau) + \hat{Q}_a(\tau) \quad (58)$$

where

$$\hat{\Phi}_v(x) = \int \frac{d^3k}{(2\pi)^3} \sqrt{\frac{\hbar}{2\omega}} \left[f^{(+)}(t, \mathbf{x}; \mathbf{k}) \hat{v}_{\mathbf{k}} + f^{(-)}(t, \mathbf{x}; \mathbf{k}) \hat{v}_{\mathbf{k}}^\dagger \right], \quad (59)$$

$$\hat{\Phi}_a(x) = \sqrt{\frac{\hbar}{2\Omega_r m_0}} \left[f^a(t, \mathbf{x}) \hat{a} + f^{a*}(t, \mathbf{x}) \hat{a}^\dagger \right], \quad (60)$$

$$\hat{Q}_v(\tau) = \int \frac{d^3k}{(2\pi)^3} \sqrt{\frac{\hbar}{2\omega}} \left[q^{(+)}(\tau, \mathbf{k}) \hat{v}_{\mathbf{k}} + q^{(-)}(\tau, \mathbf{k}) \hat{v}_{\mathbf{k}}^\dagger \right], \quad (61)$$

$$\hat{Q}_a(\tau) = \sqrt{\frac{\hbar}{2\Omega_r m_0}} \left[q^a(\tau) \hat{a} + q^{a*}(\tau) \hat{a}^\dagger \right]. \quad (62)$$

The entire problem, therefore, can be transformed by solving c -number functions $f(x)$ and $q(\tau)$ from Eq. (49) and (50) with suitable initial conditions. Since \hat{Q} and $\hat{\Phi}$ are Hermitian, one has $f^{(-)} = (f^{(+)})^*$ and $q^{(-)} = (q^{(+)})^*$. Hence, it is sufficient to solve the c -number functions $f^{(+)}(t, \mathbf{x}; \mathbf{k})$, $q^{(+)}(\tau, \mathbf{k})$, $f^a(t, \mathbf{x})$ and $q^a(\tau)$. To place this in a more general setting, let us perform a Lorentz transformation shifting $\tau = 0$ to $\tau = \tau_0$, and let us define

$$\eta \equiv \tau - \tau_0. \quad (63)$$

Now the coupling between the detector and the field would be turned on at $\tau = \tau_0$. We are looking for solutions with the initial conditions such as the following:

$$f^{(+)}(t(\tau_0), \mathbf{x}; \mathbf{k}) = e^{i\mathbf{k}\cdot\mathbf{x}}, \quad \partial_t f^{(+)}(t(\tau_0), \mathbf{x}; \mathbf{k}) = -i\omega e^{i\mathbf{k}\cdot\mathbf{x}}, \quad q^{(+)}(\tau_0; \mathbf{k}) = \dot{q}^{(+)}(\tau_0; \mathbf{k}) = 0, \quad (64)$$

$$f^a(t(\tau_0), \mathbf{x}) = \partial_t f^a(t(\tau_0), \mathbf{x}) = 0, \quad q^a(\tau_0) = 1, \quad \dot{q}^a(\tau_0) = -i\Omega_r. \quad (65)$$

The solutions for $f_0^{(+)}$, $f^{(+)}$, $q^{(+)}$, f^a , and q^a are as follows (detailed calculations for one moving detector Bob are written in Appendix C). The general solution for $f^{(+)}$ reads

$$f^{(+)}(x; \mathbf{k}) = f_0^{(+)}(x; \mathbf{k}) + f_1^{(+)}(x; \mathbf{k}), \quad (66)$$

where

$$f_0^{(+)}(x; \mathbf{k}) \equiv e^{-i\omega t + i\mathbf{k}\cdot\mathbf{x}} \quad (67)$$

is the free field solution and

$$f_1^{(+)}(z(\tau); \mathbf{k}) = \frac{\lambda_0}{4\pi} \left[\Lambda \zeta q^{(+)}(\tau; \mathbf{k}) - \partial_\tau q^{(+)}(\tau; \mathbf{k}) + O(\Lambda^{-1}) \right], \quad (68)$$

where $\zeta = 2^{7/4} \Gamma(5/4) / \sqrt{\pi}$ and Λ is about the regularization scheme.

The mode function of the internal degrees of freedom \hat{Q} about the vacuum fluctuations part is

$$q^{(+)}(\tau; \mathbf{k}) = \frac{\lambda_0}{m_0} \sum_{j=+,-} \int_{\tau_0}^{\tau} d\tau' c_j e^{w_j(\tau-\tau')} f_0^{(+)}(z(\tau'); \mathbf{k}), \quad (69)$$

where $c_{\pm} = \pm \frac{1}{2i\Omega}$, $w_{\pm} = -\gamma \pm i\Omega$, with $\Omega \equiv \sqrt{\Omega_r^2 - \gamma^2}$:

$$f^a(x) = \frac{\lambda_0 \theta(\eta_-)}{2\pi a X} q^a(\tau_-), \quad (70)$$

where X is as defined in Appendix C.

The mode functions of the internal degrees of freedom \hat{Q} about the intrinsic part are

$$q^a(\tau) = \frac{1}{2} \theta(\eta) e^{-\gamma\eta} \left[\left(1 - \frac{\Omega_r + i\gamma}{\Omega} \right) e^{i\Omega\eta} + \left(1 + \frac{\Omega_r + i\gamma}{\Omega} \right) e^{-i\Omega\eta} \right]. \quad (71)$$

Above is the general form of the solutions. The explicit solutions will depend on the specific worldline of the detector (the trajectory for the moving detector in spacetime).

As is shown above, when \hat{Q} evolves, some nonzero terms proportional to $\hat{\Phi}$ and $\hat{\Pi}$ will be generated. Suppose that the detector is initially prepared in a state that can be factorized into the quantum state $|q\rangle$ for Q and the Minkowski vacuum $|0_M\rangle$ for the scalar field Φ , that is,

$$|\tau_0\rangle = |q\rangle |0_M\rangle. \quad (72)$$

The two-point function of Q will then split into two parts,

$$\begin{aligned} \langle Q(\tau)Q(\tau') \rangle &= \langle 0_M | \langle q | \left[\hat{Q}_v(\tau) + \hat{Q}_a(\tau) \right] \left[\hat{Q}_v(\tau') + \hat{Q}_a(\tau') \right] | q \rangle | 0_M \rangle \\ &= \langle q | q \rangle \langle Q(\tau)Q(\tau') \rangle_v + \langle Q(\tau)Q(\tau') \rangle_a \langle 0_M | 0_M \rangle, \end{aligned} \quad (73)$$

where, from Eq. (58),

$$\langle Q(\tau)Q(\tau') \rangle_v = \langle 0_M | \hat{Q}_v(\tau)\hat{Q}_v(\tau') | 0_M \rangle, \quad (74)$$

$$\langle Q(\tau)Q(\tau') \rangle_a = \langle q | \hat{Q}_a(\tau)\hat{Q}_a(\tau') | q \rangle. \quad (75)$$

Similar splitting happens for every two-point function of $\hat{\Phi}(x)$.

Observe that $\langle Q(\tau)Q(\tau') \rangle_v$ depends on the initial state of the field, or the Minkowski vacuum, while $\langle Q(\tau)Q(\tau') \rangle_a$ depends on the initial state of the detector only. One can thus interpret $\langle Q(\tau)Q(\tau') \rangle_v$ as accounting for the response to the vacuum fluctuations, while $\langle Q(\tau)Q(\tau') \rangle_a$ corresponds to the intrinsic quantum fluctuations in the detector. Here we will focus on the $\langle Q(\tau)Q(\tau') \rangle_v$ part (the response to the vacuum fluctuations) and demonstrate the explicit forms of the two-point correlation functions.

APPENDIX C: SOLVING FOR $f_0^{(+)}$, $f^{(+)}$, $q^{(+)}$, f^a , AND q^a

The method for obtaining f and q is analogous to what we did in classical field theory [16]. We first find an expression relating the harmonic oscillator to the field amplitude right at the detector. Substituting this relation into the equation of motions for the oscillator, we then obtain the equation of motion for q using the information from the field. We then solve this equation of motion for q and, from its solution, determine the field f consistently.

Eq.(50) implies that

$$(\partial_t^2 - \nabla^2)f^{(+)}(x; \mathbf{k}) = \lambda_0 \int_{\tau_0}^{\infty} d\tau \delta^4(x - z(\tau)) q^{(+)}(\tau; \mathbf{k}). \quad (76)$$

The general solution for $f^{(+)}$ reads

$$f^{(+)}(x; \mathbf{k}) = f_0^{(+)}(x; \mathbf{k}) + f_1^{(+)}(x; \mathbf{k}), \quad (77)$$

where

$$f_0^{(+)}(x; \mathbf{k}) \equiv e^{-i\omega t + i\mathbf{k}\cdot\mathbf{x}} \quad (78)$$

is the free field solution and

$$f_1^{(+)}(x; \mathbf{k}) \equiv \lambda_0 \int_{\tau_0}^{\infty} d\tau G_{\text{ret}}(x; z(\tau)) q^{(+)}(\tau; \mathbf{k}) \quad (79)$$

is the retarded solution, which looks like the retarded field in classical field theory. Here $\omega = |\mathbf{k}|$ and the retarded Green's function G_{ret} in Minkowski space is given by

$$G_{\text{ret}}(x, x') = \frac{1}{4\pi} \delta(\sigma) \theta(t - t') \quad (80)$$

with $\sigma \equiv -(x_\mu - x'_\mu)(x^\mu - x'^\mu)/2$. Applying the explicit form of the retarded Green's function, one can go further to write

$$f_1^{(+)}(x; \mathbf{k}) = \frac{\lambda_0 \theta(\eta_-)}{2\pi a X} q^{(+)}(\tau_-; \mathbf{k}), \quad (81)$$

where

$$X \equiv \sqrt{(-UV + \rho^2 + a^{-2})^2 + 4a^{-2}UV}, \quad (82)$$

$$\tau_- \equiv -\frac{1}{a} \ln \frac{a}{2|V|} (X - UV + \rho^2 + a^{-2}), \quad (83)$$

$$\eta_- \equiv \tau_- - \tau_0, \quad (84)$$

with $\rho \equiv \sqrt{x_2^2 + x_3^2}$, $U \equiv t - x^1$ and $V \equiv t + x^1$.

The formal retarded solution (81) is singular on the trajectory of the detector. To deal with the singularity, note that the UAD detector here is a quantum mechanical object, and also that the detector number would always be 1. This means that at the energy threshold of detector creations, there is a natural cutoff of the frequency, which sets an upper bound on the resolution to be explored in our theory. Thus, it is justified to assume here that the detector has a finite extent $O(\Lambda^{-1})$, which will introduce the backreaction on the detector.

Let us regularize the retarded Green's function by invoking the essence of effective field theory:

$$G_{\text{ret}}^\Lambda(x, x') = \frac{1}{4\pi} \sqrt{\frac{8}{\pi}} \Lambda^2 e^{-2\Lambda^4 \sigma^2} \theta(t - t'). \quad (85)$$

(For more details on this regularization scheme, see Refs.[14, 19].) Taking this, right on the trajectory, the retarded solution for large Λ is

$$f_1^{(+)}(z(\tau); \mathbf{k}) = \frac{\lambda_0}{4\pi} \left[\Lambda \zeta q^{(+)}(\tau; \mathbf{k}) - \partial_\tau q^{(+)}(\tau; \mathbf{k}) + O(\Lambda^{-1}) \right], \quad (86)$$

where $\zeta = 2^{7/4} \Gamma(5/4) / \sqrt{\pi}$. Substituting the above expansion into Eq. (49) and neglecting the $O(\Lambda^{-1})$ terms, one obtains the following equation of motion for $q^{(+)}$ with backreaction:

$$(\partial_\tau^2 + 2\gamma \partial_\tau + \Omega_r^2) q^{(+)}(\tau; \mathbf{k}) = \frac{\lambda_0}{m_0} f_0^{(+)}(z(\tau); \mathbf{k}). \quad (87)$$

Fortunately, there is no higher derivative of q present in the above equation of motion. Now $q^{(+)}$ behaves like a damped harmonic oscillator driven by the vacuum fluctuations of the scalar field, with the damping constant

$$\gamma \equiv \frac{\lambda_0^2}{8\pi m_0}, \quad (88)$$

and the renormalized natural frequency

$$\Omega_r^2 \equiv \Omega_0^2 - \frac{\lambda_0^2 \Lambda \zeta}{4\pi m_0}. \quad (89)$$

In Eq. (87), the solution for $q^{(+)}$ compatible with the initial conditions $q^{(+)}(\tau_0; \mathbf{k}) = \dot{q}^{(+)}(\tau_0; \mathbf{k}) = 0$ is

$$q^{(+)}(\tau; \mathbf{k}) = \frac{\lambda_0}{m_0} \sum_{j=+,-} \int_{\tau_0}^{\tau} d\tau' c_j e^{w_j(\tau-\tau')} f_0^{(+)}(z(\tau'); \mathbf{k}), \quad (90)$$

where $f_0^{(+)}$ was given in Eq. (78), c_\pm and w_\pm are defined as

$$c_\pm = \pm \frac{1}{2i\Omega}, \quad w_\pm = -\gamma \pm i\Omega, \quad (91)$$

with

$$\Omega \equiv \sqrt{\Omega_r^2 - \gamma^2}. \quad (92)$$

Throughout this paper we consider only the underdamped case with $\gamma^2 < \Omega_r^2$, so Ω is always real.

Similarly, from Eq. (49), (50), (57) and (58), the equations of motion for f^a and q^a read

$$(\partial_t^2 - \nabla^2) f^a(x) = \lambda_0 \int d\tau \delta^4(x - z(\tau)) q^a(\tau), \quad (93)$$

$$(\partial_\tau^2 + \Omega_0^2) q^a(\tau) = \frac{\lambda_0}{m_0} f^a(z(\tau)). \quad (94)$$

The general solution for f^a , as in Eq. (77), is

$$f^a(x) = f_0^a(x) + \lambda_0 \int_{\tau_0}^{\infty} d\tau G_{\text{ret}}(x; z(\tau)) q^a(\tau_-). \quad (95)$$

However, according to the initial condition (65), one has $f_0^a = 0$; hence,

$$f^a(x) = \frac{\lambda_0 \theta(\eta_-)}{2\pi a X} q^a(\tau_-). \quad (96)$$

Again, the value of f^a is singular right at the position of the detector. Performing the same regularization as was given for $q^{(+)}$, Eq.(94) becomes

$$(\partial_\tau^2 + 2\gamma\partial_\tau + \Omega_r^2) q^a(\tau) = 0, \quad (97)$$

which describes a damped harmonic oscillator free of driving force. The solution consistent with the initial condition $q^a(\tau_0) = 1$ and $\dot{q}^b(\tau_0) = -i\Omega_r$ reads

$$q^a(\tau) = \frac{1}{2} \theta(\eta) e^{-\gamma\eta} \left[\left(1 - \frac{\Omega_r + i\gamma}{\Omega}\right) e^{i\Omega\eta} + \left(1 + \frac{\Omega_r + i\gamma}{\Omega}\right) e^{-i\Omega\eta} \right]. \quad (98)$$

APPENDIX D: THE INTEGRATION OF κ

$$\begin{aligned} & \langle Q(\tau - \tau_0) Q(\tau'' - \tau_0'') \rangle_v \\ &= \frac{\lambda_0^2 \hbar}{2m_0^2 (2\pi)^2} \left[\sum_{j,j'=\pm} C_j C_{j'}^* \int_{-\infty}^{\infty} \frac{\kappa d\kappa e^{-i\kappa(\tau_0 - \tau_0'')} (e^{w_j(\tau - \tau_0)} - e^{i\kappa(\tau_0 - \tau)}) (e^{w_{j'}^*(\tau'' - \tau_0'')} - e^{i\kappa(\tau'' - \tau_0'')})}{(1 - e^{-2\pi\kappa/a})(w_j + i\kappa)(w_{j'}^* - i\kappa)} \right. \\ & \quad \left. - \sum_{j,j'=\pm} C_j C_{j'}^* \int_{-\infty}^0 \frac{\kappa d\kappa e^{-i\kappa(\tau_0 - \tau_0'')} (e^{w_j(\tau - \tau_0)} - e^{i\kappa(\tau_0 - \tau)}) (e^{w_{j'}^*(\tau'' - \tau_0'')} - e^{i\kappa(\tau'' - \tau_0'')})}{(w_j + i\kappa)(w_{j'}^* - i\kappa)} \right] \\ &= \langle QQ \rangle_{v1} - \langle QQ \rangle_{v2}, \end{aligned} \quad (99)$$

$$\begin{aligned} & \langle QQ \rangle_{v1} \\ &= \frac{\lambda_0^2 \hbar}{2m_0^2 (2\pi)^2} \sum_{j,j'=\pm} C_j C_{j'}^* \int_{-\infty}^{\infty} \frac{\kappa d\kappa e^{-i\kappa(\tau_0 - \tau_0'')} (e^{w_j(\tau - \tau_0)} - e^{i\kappa(\tau_0 - \tau)}) (e^{w_{j'}^*(\tau'' - \tau_0'')} - e^{i\kappa(\tau'' - \tau_0'')})}{(1 - e^{-2\pi\kappa/a})(w_j + i\kappa)(w_{j'}^* - i\kappa)} \\ &= \frac{\lambda_0^2 \hbar}{2m_0^2 (2\pi)^2} \sum_{j,j'=\pm} \frac{C_j C_{j'}^*}{w_j + w_{j'}^*} \int_{-\infty}^{\infty} \frac{d\kappa}{1 - e^{-2\pi\kappa/a}} \left(\frac{w_j}{\kappa - iw_j} + \frac{w_{j'}^*}{\kappa + iw_{j'}^*} \right) (e_1 + e_2 + e_3 + e_4) \\ &= P_1 + P_2 + P_3 + P_4, \end{aligned} \quad (100)$$

$$e_1 = e^{-i\kappa(\tau_0 - \tau_0'') + w_j(\tau - \tau_0) + w_{j'}^*(\tau'' - \tau_0'')}, \quad (101)$$

$$e_2 = -e^{w_j(\tau-\tau_0)+i\kappa(\tau''-\tau_0)}, \quad (102)$$

$$e_3 = -e^{w_{j'}^*(\tau''-\tau_0')-i\kappa(\tau-\tau_0')}, \quad (103)$$

$$e_4 = e^{i\kappa(\tau''-\tau)}. \quad (104)$$

where

$$\begin{aligned} P_1 &= \frac{\lambda_0^2 \hbar}{2m_0^2(2\pi)^2} \sum_{j,j'=\pm} \frac{C_j C_{j'}^*}{w_j + w_{j'}} \int_{-\infty}^{\infty} \frac{d\kappa}{1 - e^{-2\pi\kappa/a}} \left(\frac{w_j}{\kappa - iw_j} + \frac{w_{j'}^*}{\kappa + iw_{j'}^*} \right) e^{-i\kappa(\tau_0-\tau_0') + w_j(\tau-\tau_0) + w_{j'}^*(\tau''-\tau_0')} \\ &= \frac{\lambda_0^2 \hbar}{2m_0^2(2\pi)^2} \sum_{j,j'=\pm} \frac{C_j C_{j'}^*}{w_j + w_{j'}} e^{w_j(\tau-\tau_0) + w_{j'}^*(\tau''-\tau_0')} \cdot (-2\pi i) \cdot \\ &\quad \left[\frac{a}{2\pi} \sum_{n=-\infty}^{-1} \left(\frac{w_j}{ina - iw_j} + \frac{w_{j'}^*}{ina + iw_{j'}^*} \right) e^{-na(\tau_0-\tau_0')} + \frac{w_j e^{w_j(\tau_0-\tau_0')}}{1 - e^{-2i\pi w_j^*/a}} \right] \\ &= \frac{\lambda_0^2 \hbar}{2m_0^2(2\pi)^2} \sum_{j,j'=\pm} \frac{C_j C_{j'}^*}{w_j + w_{j'}} e^{w_j(\tau-\tau_0) + w_{j'}^*(\tau''-\tau_0')} \cdot \\ &\quad \left[\frac{w_j e^{-a(\tau_0-\tau_0')}}{1 + w_j/a} F_{w_j}(e^{-a(\tau_0-\tau_0')}) + \frac{w_{j'}^* e^{-a(\tau_0-\tau_0')}}{1 - w_{j'}^*/a} F_{-w_{j'}^*}(e^{-a(\tau_0-\tau_0')}) - \frac{2\pi i w_j e^{w_j(\tau_0-\tau_0')}}{1 - e^{-2i\pi w_j/a}} \right]. \end{aligned} \quad (105)$$

$$\begin{aligned} P_2 &= \frac{-\lambda_0^2 \hbar}{2m_0^2(2\pi)^2} \sum_{j,j'=\pm} \frac{C_j C_{j'}^*}{w_j + w_{j'}^*} \int_{-\infty}^{\infty} \frac{d\kappa}{1 - e^{-2\pi\kappa/a}} \left(\frac{w_j}{\kappa - iw_j} + \frac{w_{j'}^*}{\kappa + iw_{j'}^*} \right) e^{w_j(\tau-\tau_0) + i\kappa(\tau''-\tau_0)} \\ &= \frac{-\lambda_0^2 \hbar}{2m_0^2(2\pi)^2} \sum_{j,j'=\pm} \frac{C_j C_{j'}^*}{w_j + w_{j'}^*} e^{w_j(\tau-\tau_0)} \cdot (2\pi i) \cdot \\ &\quad \left[\frac{a}{2\pi} \sum_0^{\infty} \left(\frac{w_j}{ina - iw_j} + \frac{w_{j'}^*}{ina + iw_{j'}^*} \right) e^{-na(\tau''-\tau_0)} + \frac{w_{j'}^* e^{w_{j'}^*(\tau''-\tau_0)}}{1 - e^{2i\pi w_{j'}^*/a}} \right] \\ &= \frac{-\lambda_0^2 \hbar}{2m_0^2(2\pi)^2} \sum_{j,j'=\pm} \frac{C_j C_{j'}^*}{w_j + w_{j'}^*} e^{w_j(\tau-\tau_0)} \cdot \left[\frac{w_j e^{-a(\tau''-\tau_0)}}{1 - w_j/a} F_{-w_j}(e^{-a(\tau''-\tau_0)}) \right. \\ &\quad \left. + \frac{w_{j'}^* e^{-a(\tau''-\tau_0)}}{1 + w_{j'}^*/a} F_{w_{j'}^*}(e^{-a(\tau''-\tau_0)}) + \frac{2\pi i w_{j'}^* e^{w_{j'}^*(\tau''-\tau_0)}}{1 - e^{2i\pi w_{j'}^*/a}} \right]. \end{aligned} \quad (106)$$

Since $e_3 = e_2^* |_{\tau \leftrightarrow \tau', \tau_0 \leftrightarrow \tau_0'}$, we have $P_3 = P_2^* |_{\tau \leftrightarrow \tau', \tau_0 \leftrightarrow \tau_0'}$. And

$$\begin{aligned} P_4 &= \frac{\lambda_0^2 \hbar}{2m_0^2(2\pi)^2} \sum_{j,j'=\pm} \frac{C_j C_{j'}^*}{w_j + w_{j'}^*} \cdot \left[\frac{w_j e^{-a(\tau_0-\tau_0')}}{1 + w_j/a} F_{w_j}(e^{-a(\tau_0-\tau_0')}) \right. \\ &\quad \left. + \frac{w_{j'}^* e^{-a(\tau_0-\tau_0')}}{1 - w_{j'}^*/a} F_{-w_{j'}^*}(e^{-a(\tau_0-\tau_0')}) - \frac{2\pi i w_{j'} e^{w_j(\tau_0-\tau_0')}}{1 - e^{-2i\pi w_j/a}} \right]. \end{aligned} \quad (107)$$

we use the following formula to show our results:

$$\sum_{n=1}^{\infty} \frac{e^{-nx}}{n+y} = \frac{e^{-x}}{1+y} {}_2F_1(1+y, 1, 2+y, e^{-x}) \equiv \frac{e^{-x}}{1+y} F_{ay}(e^{-x}). \quad (108)$$

When we combine P_1, P_2, P_3 and P_4 and define $\eta \equiv \tau - \tau_0$, $\eta'' \equiv \tau'' - \tau_0''$, the two point function $\langle Q(\eta)Q(\eta'') \rangle_{v1}$ is

$$\langle Q(\eta), Q(\eta'') \rangle_{v1} \equiv \frac{1}{2} \langle Q(\eta)Q(\eta'') + Q(\eta'')Q(\eta) \rangle_{v1} = \text{Re}\{P_1 + P_2 + P_3 + P_4\} \quad (109)$$

$$\begin{aligned} \langle Q(\eta)^2 \rangle_{v1} &\equiv \lim_{\eta'' \rightarrow \eta} \frac{1}{2} \langle \{Q(\eta), Q(\eta'')\} \rangle_{v1} = \lim_{\eta'' \rightarrow \eta} \text{Re}\{P_1 + P_2 + P_3 + P_4\} \\ &= \frac{\hbar\gamma}{\pi m_0 \Omega^2} \theta(\eta) \text{Re}\left\{ \left(\Lambda_0 - \ln \frac{a}{\Omega} \right) e^{-2\gamma\eta} \sin^2 \Omega\eta \right. \\ &\quad \left. + \frac{a}{2} e^{-(\gamma+a)\eta} \left[\frac{F_{\gamma+i\Omega}(e^{-a\eta})}{\gamma+i\Omega+a} \left(\frac{-i\Omega}{\gamma} \right) e^{-i\Omega\eta} + \frac{F_{-\gamma-i\Omega}(e^{-a\eta})}{\gamma+i\Omega-a} \left(\left(1 + \frac{i\Omega}{\gamma} \right) e^{i\Omega\eta} - e^{-i\Omega\eta} \right) \right] \right. \\ &\quad \left. - \frac{1}{4} \left[\left(\frac{i\Omega}{\gamma} + e^{-2\gamma\eta} \left(\frac{i\Omega}{\gamma} + 1 - e^{-2i\Omega\eta} \right) \right) (\psi_{\gamma+i\Omega} + \psi_{-\gamma-i\Omega}) \right. \right. \\ &\quad \left. \left. - \left(\frac{-i\Omega}{\gamma} + e^{-2\gamma\eta} \left(\frac{i\Omega}{\gamma} + 1 - e^{-2i\Omega\eta} \right) \right) i\pi \coth \frac{\pi}{a} (\Omega - i\gamma) \right] \right\}. \end{aligned} \quad (110)$$

Here $\psi_s \equiv \psi(1 + \frac{s}{a})$ and $\Lambda_0 \equiv -\gamma_E - \ln \Omega |\tau_0 - \tau_0''|$ as $\eta' \rightarrow \eta$

$$\begin{aligned} &-\langle QQ \rangle_{v2} \\ &= \frac{-\lambda_0^2 \hbar}{2m_0^2 (2\pi)^2} \sum_{j, j' = \pm} c_j c_{j'}^* \int_{-\infty}^0 \frac{\kappa d\kappa e^{-i\kappa(\tau_0 - \tau_0'')} (e^{w_j(\tau - \tau_0)} - e^{i\kappa(\tau_0 - \tau)}) (e^{w_{j'}^*(\tau'' - \tau_0'')} - e^{i\kappa(\tau'' - \tau_0'')})}{(w_j + i\kappa)(w_{j'}^* - i\kappa)} \\ &= \frac{-\lambda_0^2 \hbar}{2m_0^2 (2\pi)^2} \sum_{j, j' = \pm} \frac{c_j c_{j'}^*}{w_j + w_{j'}^*} \int_{-\infty}^0 d\kappa \left(\frac{w_j}{\kappa - iw_j} + \frac{w_{j'}^*}{\kappa + iw_{j'}^*} \right) (e_1 + e_2 + e_3 + e_4) \\ &= -\tilde{P}_1 - \tilde{P}_2 - \tilde{P}_3 - \tilde{P}_4, \end{aligned} \quad (111)$$

$$\begin{aligned} \tilde{P}_1 &= \frac{\lambda_0^2 \hbar}{2m_0^2 (2\pi)^2} \sum_{j, j' = \pm} \frac{c_j c_{j'}^*}{w_j + w_{j'}^*} \int_{-\infty}^0 d\kappa \left(\frac{w_j}{\kappa - iw_j} + \frac{w_{j'}^*}{\kappa + iw_{j'}^*} \right) e^{-i\kappa(\tau_0 - \tau_0'') + w_j(\tau - \tau_0) + w_{j'}^*(\tau'' - \tau_0'')} \\ &= \frac{\lambda_0^2 \hbar}{2m_0^2 (2\pi)^2} \left[\left(\frac{c_+ c_+^*}{w_+ + w_+^*} w_+ e^{w_+(\tau - \tau_0'') + w_+^*(\tau'' - \tau_0'')} + \frac{c_+ c_-^*}{w_+ + w_-^*} w_+ e^{w_+(\tau - \tau_0'') + w_-^*(\tau'' - \tau_0'')} \right) \right. \\ &\quad \cdot (-i2\pi - \Gamma(0, w_+(\tau_0 - \tau_0'')) + \log(w_+) + \log(\tau_0 - \tau_0'') - \log(w_+(\tau_0 - \tau_0''))) \\ &\quad \left. + \left(\frac{c_- c_+^*}{w_- + w_+^*} w_- e^{w_-(\tau - \tau_0'') + w_+^*(\tau'' - \tau_0'')} + \frac{c_- c_-^*}{w_- + w_-^*} w_- e^{w_-(\tau - \tau_0'') + w_-^*(\tau'' - \tau_0'')} \right) \right. \\ &\quad \cdot (-\Gamma(0, w_-(\tau_0 - \tau_0'')) + \log(w_-) + \log(\tau_0 - \tau_0'') - \log(w_-(\tau_0 - \tau_0''))) \\ &\quad \left. - \left(\frac{c_+ c_+^*}{w_+ + w_+^*} w_+^* e^{w_+(\tau - \tau_0) + w_+^*(\tau'' - \tau_0)} + \frac{c_- c_+^*}{w_- + w_+^*} w_+^* e^{w_-(\tau - \tau_0) + w_+^*(\tau'' - \tau_0)} \right) \right. \\ &\quad \cdot (\Gamma(0, -w_+^*(\tau_0 - \tau_0'')) + \log(-1/w_+^*) - \log(\tau_0 - \tau_0'') + \log(-w_+^*(\tau_0 - \tau_0''))) \\ &\quad \left. - \left(\frac{c_+ c_-^*}{w_+ + w_-^*} w_-^* e^{w_+(\tau - \tau_0) + w_-^*(\tau'' - \tau_0)} + \frac{c_- c_-^*}{w_- + w_-^*} w_-^* e^{w_-(\tau - \tau_0) + w_-^*(\tau'' - \tau_0)} \right) \right. \\ &\quad \left. \cdot (\Gamma(0, -w_-^*(\tau_0 - \tau_0'')) + \log(-1/w_-^*) - \log(\tau_0 - \tau_0'') + \log(-w_-^*(\tau_0 - \tau_0''))) \right], \end{aligned} \quad (112)$$

$$\begin{aligned} \tilde{P}_2 &= \frac{\lambda_0^2 \hbar}{2m_0^2 (2\pi)^2} \sum_{j, j' = \pm} \frac{c_j c_{j'}^*}{w_j + w_{j'}^*} \int_{-\infty}^0 d\kappa \left(\frac{w_j}{\kappa - iw_j} + \frac{w_{j'}^*}{\kappa + iw_{j'}^*} \right) e_2 \\ &= \frac{-\lambda_0^2 \hbar}{2m_0^2 (2\pi)^2} \left[- \left(\frac{c_+ c_+^*}{w_+ + w_+^*} + \frac{c_+ c_-^*}{w_+ + w_-^*} \right) w_+ e^{w_+(\tau - \tau'')} \right] \end{aligned}$$

$$\begin{aligned}
& \cdot (\Gamma(0, -w_+(\tau'' - \tau_0)) + \log(-1/w_+) + \log(-w_+(\tau'' - \tau_0)) - \log(\tau'' - \tau_0)) \\
& - \left(\frac{c_- c_+^*}{w_- + w_+^*} + \frac{c_- c_-^*}{w_- + w_-^*} \right) w_- e^{w_-(\tau - \tau'')} \\
& \cdot (\Gamma(0, -w_-(\tau'' - \tau_0)) + \log(-1/w_-) + \log(-w_-(\tau'' - \tau_0)) - \log(\tau'' - \tau_0)) \\
& + \left(\frac{c_+ c_+^*}{w_+ + w_+^*} w_+^* e^{w_+(\tau - \tau_0)} + \frac{c_- c_+^*}{w_- + w_+^*} w_+^* e^{w_-(\tau - \tau_0)} \right) e^{w_+(\tau'' - \tau_0)} \\
& \cdot (2\pi i - \Gamma(0, w_+(\tau'' - \tau_0)) + \log(w_+) - \log(w_+(\tau'' - \tau_0)) + \log(\tau'' - \tau_0)) \\
& - \left(\frac{c_+ c_-^*}{w_+ + w_-^*} w_-^* e^{w_+(\tau - \tau_0)} + \frac{c_- c_-^*}{w_- + w_-^*} w_-^* e^{w_-(\tau - \tau_0)} \right) e^{w_-(\tau'' - \tau_0)} \\
& \cdot (\Gamma(0, w_-(\tau'' - \tau_0)) - \log(w_-) + \log(w_-(\tau'' - \tau_0)) - \log(\tau'' - \tau_0)) \Big] , \tag{113}
\end{aligned}$$

$$\begin{aligned}
\tilde{P}_3 &= \frac{\lambda_0^2 \hbar}{2m_0^2 (2\pi)^2} \sum_{j, j' = \pm} \frac{c_j c_{j'}^*}{w_j + w_{j'}^*} \int_{-\infty}^0 d\kappa \left(\frac{w_j}{\kappa - iw_j} + \frac{w_{j'}^*}{\kappa + iw_{j'}^*} \right) e_3 \\
&= \frac{-\lambda_0^2 \hbar}{2m_0^2 (2\pi)^2} \left[-e^{w_+(\tau - \tau_0'')} \left(\frac{c_+ c_+^*}{w_+ + w_+^*} w_+ e^{w_+(\tau'' - \tau_0'')} + \frac{c_+ c_-^*}{w_+ + w_-^*} w_+ e^{w_-(\tau'' - \tau_0'')} \right) \right. \\
&\quad \cdot (-2\pi i + \Gamma(0, w_+(\tau - \tau_0'')) - \log(w_+) - \log(\tau - \tau_0'') + \log(w_+(\tau - \tau_0''))) \\
&\quad - e^{w_-(\tau - \tau_0'')} \left(\frac{c_- c_+^*}{w_- + w_+^*} w_- e^{w_+(\tau'' - \tau_0'')} + \frac{c_- c_-^*}{w_- + w_-^*} w_- e^{w_-(\tau'' - \tau_0'')} \right) \\
&\quad \cdot (\Gamma(0, w_-(\tau - \tau_0'')) - \log(w_-) - \log(\tau - \tau_0'') + \log(w_-(\tau - \tau_0''))) \\
&\quad - \left(\frac{c_+ c_+^*}{w_+ + w_+^*} w_+^* e^{w_+(\tau'' - \tau)} + \frac{c_- c_+^*}{w_- + w_+^*} w_+^* e^{w_+(\tau'' - \tau)} \right) \\
&\quad \cdot (\Gamma(0, -w_+(\tau - \tau_0'')) + \log(-1/w_+) - \log(\tau - \tau_0'') + \log(-w_+(\tau - \tau_0''))) \\
&\quad - \left(\frac{c_+ c_-^*}{w_+ + w_-^*} w_-^* e^{w_-(\tau'' - \tau)} + \frac{c_- c_-^*}{w_- + w_-^*} w_-^* e^{w_-(\tau'' - \tau)} \right) \\
&\quad \cdot (\Gamma(0, -w_-(\tau - \tau_0'')) + \log(-1/w_-) - \log(\tau - \tau_0'') + \log(-w_-(\tau - \tau_0''))) \Big] , \tag{114}
\end{aligned}$$

$$\begin{aligned}
\tilde{P}_4 &= \frac{\lambda_0^2 \hbar}{2m_0^2 (2\pi)^2} \sum_{j, j' = \pm} \frac{c_j c_{j'}^*}{w_j + w_{j'}^*} \int_{-\infty}^0 d\kappa \left(\frac{w_j}{\kappa - iw_j} + \frac{w_{j'}^*}{\kappa + iw_{j'}^*} \right) e_4 \\
&= \frac{\lambda_0^2 \hbar}{2m_0^2 (2\pi)^2} \left[- \left(\frac{c_+ c_+^*}{w_+ + w_+^*} + \frac{c_+ c_-^*}{w_+ + w_-^*} \right) w_+ e^{-w_+(\tau'' - \tau)} \right. \\
&\quad \cdot (\Gamma(0, -w_+(\tau'' - \tau)) + \log(-1/w_+) - \log(\tau'' - \tau) + \log(-w_+(\tau'' - \tau))) \\
&\quad - \left(\frac{c_- c_+^*}{w_- + w_+^*} + \frac{c_- c_-^*}{w_- + w_-^*} \right) w_- e^{-w_-(\tau'' - \tau)} \\
&\quad \cdot (\Gamma(0, -w_-(\tau'' - \tau)) + \log(-1/w_-) - \log(\tau'' - \tau) + \log(-w_-(\tau'' - \tau))) \\
&\quad + \left(\frac{c_+ c_+^*}{w_+ + w_+^*} + \frac{c_- c_+^*}{w_- + w_+^*} \right) w_+^* e^{w_+(\tau'' - \tau)} \\
&\quad \cdot (2\pi i - \Gamma(0, w_+(\tau'' - \tau)) + \log(w_+) + \log(\tau'' - \tau) - \log(w_+(\tau'' - \tau))) \\
&\quad - \left(\frac{c_+ c_-^*}{w_+ + w_-^*} + \frac{c_- c_-^*}{w_- + w_-^*} \right) w_-^* e^{w_-(\tau'' - \tau)} \\
&\quad \cdot (\Gamma(0, w_-(\tau'' - \tau)) - \log(w_-) - \log(\tau'' - \tau) + \log(w_-(\tau'' - \tau))) \Big] . \tag{115}
\end{aligned}$$

As $\eta \rightarrow \eta''$ (that is, $\tau'' \rightarrow \tau$ and $\tau_0'' \rightarrow \tau_0$),

$$-\langle Q^2(\eta) \rangle_{v2} = - \lim_{\eta'' \rightarrow \eta} \langle \{Q(\eta), Q(\eta'')\} \rangle_{v2} = - \lim_{\eta'' \rightarrow \eta} \text{Re} \{ \tilde{P}_1 + \tilde{P}_2 + \tilde{P}_3 + \tilde{P}_4 \}$$

$$\begin{aligned}
&= \frac{\lambda_0^2 \hbar}{2m_0^2 (2\pi)^2} \theta(\eta) \text{Re} \{ \Lambda_{0_{v_2}} - \left(\frac{\gamma - i\Omega}{8\Omega^2 \gamma} e^{-2\gamma(\tau - \tau_0)} - \frac{1}{8\Omega^2} e^{-2\gamma(\tau - \tau_0) + 2i\Omega(\tau - \tau_0)} \right) \right. \\
&\cdot \left(-2i\pi + \log(-\gamma + i\Omega) - \log\left(\frac{1}{\gamma - i\Omega}\right) \right) - \left(\frac{\gamma + i\Omega}{8\Omega^2 \gamma} e^{-2\gamma(\tau - \tau_0)} - \frac{1}{8\Omega^2} e^{-2\gamma(\tau - \tau_0) - 2i\Omega(\tau - \tau_0)} \right) \\
&\cdot \left(\log(-\gamma - i\Omega) + \log\left(\frac{1}{\gamma + i\Omega}\right) \right) + \left(\frac{-\gamma + i\Omega}{8\Omega^2 \gamma} + \frac{1}{8\Omega^2} \right) \cdot [\Gamma(0, (\gamma - i\Omega)(\tau - \tau_0)) \\
&- \log(\gamma - i\Omega) - \log(\tau - \tau_0) + \log((\gamma - i\Omega)(\tau - \tau_0))] + \left(\frac{-\gamma - i\Omega}{8\Omega^2 \gamma} + \frac{1}{8\Omega^2} \right) \\
&\cdot [\Gamma(0, (\gamma + i\Omega)(\tau - \tau_0)) - \log(\gamma + i\Omega) - \log(\tau - \tau_0) + \log((\gamma + i\Omega)(\tau - \tau_0))] \\
&+ \left(\frac{\gamma + i\Omega}{8\Omega^2 \gamma} e^{-2\gamma(\tau - \tau_0)} - \frac{1}{8\Omega^2} e^{-2(\gamma + i\Omega)(\tau - \tau_0)} \right) \cdot [2\pi i - \Gamma(0, (-\gamma - i\Omega)(\tau - \tau_0)) + \log(-\gamma - i\Omega) \\
&+ \log(\tau - \tau_0) - \log((- \gamma - i\Omega)(\tau - \tau_0))] + \left(\frac{-\gamma + i\Omega}{8\Omega^2 \gamma} e^{-2\gamma(\tau - \tau_0)} + \frac{1}{8\Omega^2} e^{2(-\gamma + i\Omega)(\tau - \tau_0)} \right) \\
&\cdot [\Gamma(0, (-\gamma + i\Omega)(\tau - \tau_0)) - \log(-\gamma + i\Omega) - \log(\tau - \tau_0) + \log((- \gamma + i\Omega)(\tau - \tau_0))] \\
&+ \left(\frac{-\gamma + i\Omega}{8\Omega^2 \gamma} e^{-2\gamma(\tau - \tau_0)} + \frac{1}{8\Omega^2} e^{2(-\gamma + i\Omega)(\tau - \tau_0)} \right) \cdot [2\pi i + \Gamma(0, (-\gamma + i\Omega)(\tau - \tau_0)) - \log(-\gamma + i\Omega) \\
&- \log(\tau - \tau_0) + \log((- \gamma + i\Omega)(\tau - \tau_0))] + \left(\frac{-\gamma - i\Omega}{8\Omega^2 \gamma} e^{-2\gamma(\tau - \tau_0)} + \frac{1}{8\Omega^2} e^{-2(\gamma + i\Omega)(\tau - \tau_0)} \right) \\
&\cdot [\Gamma(0, (-\gamma - i\Omega)(\tau - \tau_0)) - \log(-\gamma - i\Omega) - \log(\tau - \tau_0) + \log((- \gamma - i\Omega)(\tau - \tau_0))] \\
&+ \frac{i}{8\Omega \gamma} \cdot [-\Gamma(0, (\gamma + i\Omega)(\tau - \tau_0)) + \log(\gamma + i\Omega) + \log(\tau - \tau_0) - \log((\gamma + i\Omega)(\tau - \tau_0))] \\
&+ \Gamma(0, (\gamma - i\Omega)(\tau - \tau_0)) - \log(\gamma - i\Omega) - \log(\tau - \tau_0) + \log((\gamma - i\Omega)(\tau - \tau_0))] \\
&+ \left(\frac{1}{8\Omega^2} - \frac{(\gamma - i\Omega)}{8\Omega^2 \gamma} \right) \cdot (-\log(\gamma - i\Omega) - \log(-\gamma - i\Omega)) + \left(\frac{1}{8\Omega^2} - \frac{(\gamma + i\Omega)}{8\Omega^2 \gamma} \right) \\
&\cdot (-2\log(\gamma + i\Omega) - 2\pi i) \}, \tag{116}
\end{aligned}$$

where $\Lambda_{0_{v_2}}$ contains the divergent parts $\Gamma(0, 0)$ and $\log(0)$ as $\tau'' \rightarrow \tau$ and $\tau_0'' \rightarrow \tau_0$ and is absorbed into the renormalized constant or coefficient in the experiment.

-
- [1] W. G. Unruh, Phys. Rev. **D 14**, 870(1976).
 - [2] P. G. Grove, Classical Quantum Gravity **3**, 801(1986).
 - [3] D. J. Raine, D. W. Sciama and P.G. Grove, Proc. R. Soc. **A 435**, 205(1991).
 - [4] W. G. Unruh, Phys. Rev. **D 46**, 3271(1992).
 - [5] S. Massar, R. Parentani and R. Brout, Classical Quantum Gravity **10**, 385(1993).
 - [6] S. Takagi, Proc. Theor. Phys. Suppl. **88**, 1(1986); V. L. Ginzburg and V. P. Frolov, Sov. Phys. Usp. **30**, 1073(1988).
 - [7] F. Hinterleitner, Ann. Phys. (N.Y.) **226**, 165(1993).
 - [8] J. Audretsch and R. Müller, Phys. Rev. **D 49**, 4056(1994); J. Audretsch, R. Müller and M. Holzmann, Phys. Lett. **A199**, 151(1995).
 - [9] S. Massar and R. Parentani, Phys. Rev. **D 54**, 7426 (1996).
 - [10] B. L. Hu and A. Raval, arXiv:quant-ph/0012135.
 - [11] A. Raval, Ph. D. thesis, University of Maryland-College Park, 1996.
 - [12] A. Raval, B. L. Hu, and J. Anglin, Phys. Rev. **D 53**, 7003(1996).
 - [13] A. Raval, B. L. Hu, and D. Koks, Phys. Rev. **D 55**, 4795(1997).
 - [14] P.R. Johnson and B. L. Hu, Phys. Rev. **D 65**, 065015 (2002).
 - [15] S.-Y. Lin, Phys. Rev. **D 68**, 104019(2003).
 - [16] S.-Y. Lin and B. L. Hu, Phys. Rev. **D 73**, 124018 (2006).
 - [17] S.-Y. Lin, Chung-Hsien Chou and B. L. Hu, Phys. Rev. **D 78**, 125025 (2008).
 - [18] S.-Y. Lin, Chung-Hsien Chou and B. L. Hu, Phys. Rev. **D 91**, 084063 (2015).
 - [19] C. R. Galley and B. L. Hu, Phys. Rev. **D72**, 084023 (2005); C. R. Galley, B. L. Hu and S.-Y. Lin, Phys. Rev. **D74**, 024017 (2006) .